TITLE:

RNF168 E3 ligase participates in ubiquitin signaling and recruitment of SLX4 during DNA crosslink repair

AUTHOR(S):

Katsuki, Yoko; Abe, Masako; Park, Seon Young; Wu, Wenwen; Yabe, Hiromasa; Yabe, Miharu; van Attikum, Haico; ... Seidman, Michael M.; Kim, Yonghwan; Takata, Minoru

京都大学学術情報リポジトリ
KURENAI 紅
Kyoto University Research Information Repository

RNF168 E3 ligase participates in ubiquitin signaling and recruitment of SLX4 during DNA crosslink repair

Graphical abstract

Highlights

- The N-terminal half of SLX4 forms foci and acts in DNA ICL damage repair

- An siRNA screen implicates RNF168 in MMC-induced GFP-SLX4-N foci formation

- Key FA pathway genes such as FANCD2 are dispensable for recruitment of SLX4

- RNF168 promotes ICL damage tolerance by tethering SLX4 by ubiquitin signaling
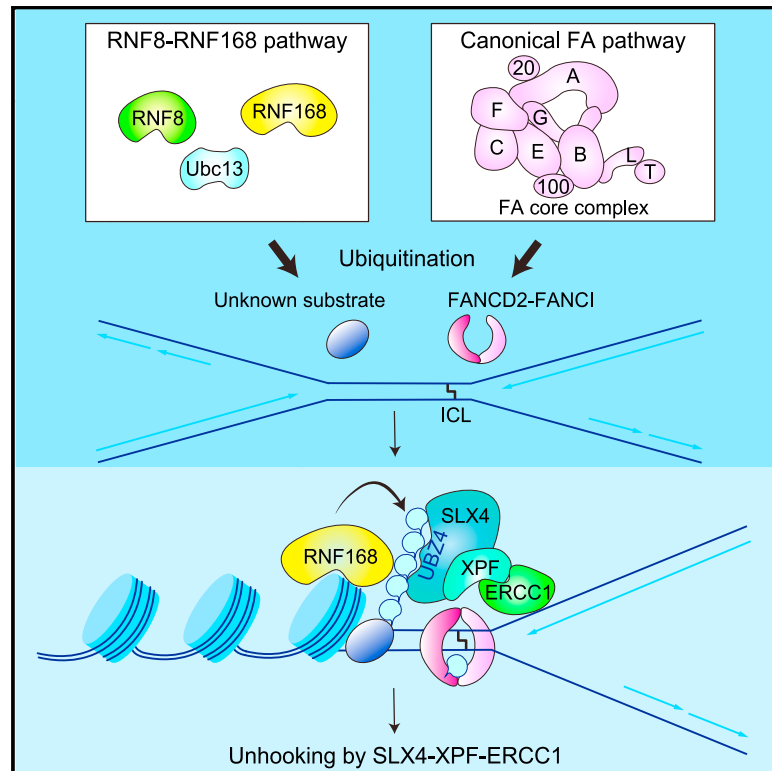
Authors

Yoko Katsuki, Masako Abe,
Seon Young Park, ..., Michael M. Seidman,
Yonghwan Kim, Minoru Takata

Correspondence

katsuki.yoko.3u@kyoto-u.ac.jp (Y.K.),
takata.minoru.8s@kyoto-u.ac.jp (M.T.)

In brief

How ubiquitin signaling mediates SLX4 localization at DNA interstrand crosslink (ICL) sites has been unclear. Katsuki et al. show that RNF168 E3 ligase contributes to an ICL-triggered ubiquitin cascade, which is required for SLX4 recruitment. Although SLX4/FANCP is an FA protein, RNF168 operates independently of the canonical FA pathway activation.

CellPress

Cell Reports

Article

RNF168 E3 ligase participates in ubiquitin signaling and recruitment of SLX4 during DNA crosslink repair

Yoko Katsuki,[1,*] Masako Abe,[2,10] Seon Young Park,[3] Wenwen Wu,[4] Hiromasa Yabe,[5] Miharu Yabe,[5] Haico van Attikum,[6] Shinichiro Nakada,[7,8] Tomohiko Ohta,[4] Michael M. Seidman,[9] Yonghwan Kim,[3] and Minoru Takata[1,11,*]

[1]Laboratory of DNA Damage Signaling, Department of Late Effects Studies, Radiation Biology Center, Graduate School of Biostudies, Kyoto University, Kyoto, Japan
[2]The Core Facility, Radiation Biology Center, Graduate School of Biostudies, Kyoto University, Kyoto, Japan
[3]Department of Biological Sciences, Sookmyung Women's University, Seoul, Republic of Korea
[4]Department of Translational Oncology, St. Marianna University Graduate School of Medicine, Kawasaki, Japan
[5]Department of Innovative Medical Science, Tokai University School of Medicine, Isehara, Japan
[6]Department of Human Genetics, Leiden University Medical Center, Leiden, the Netherlands
[7]Department of Bioregulation and Cellular Response, Graduate School of Medicine, Osaka University, Osaka, Japan
[8]Institute for Advanced Co-Creation Studies, Osaka University, Osaka, Japan
[9]Laboratory of Molecular Biology and Immunology, National Institute on Aging, National Institutes of Health, Baltimore, MD, USA
[10]Present address: Division of Advanced Biomedicine, Medical Research Support Center, Graduate School of Medicine, Kyoto University, Kyoto, Japan
[11]Lead contact
*Correspondence: katsuki.yoko.3u@kyoto-u.ac.jp (Y.K.), takata.minoru.8s@kyoto-u.ac.jp (M.T.)
https://doi.org/10.1016/j.celrep.2021.109879

SUMMARY

SLX4/FANCP is a key Fanconi anemia (FA) protein and a DNA repair scaffold for incision around a DNA interstrand crosslink (ICL) by its partner XPF nuclease. The tandem UBZ4 ubiquitin-binding domains of SLX4 are critical for the recruitment of SLX4 to damage sites, likely by binding to K63-linked polyubiquitin chains. However, the identity of the ubiquitin E3 ligase that mediates SLX4 recruitment remains unknown. Using small interfering RNA (siRNA) screening with a GFP-tagged N-terminal half of SLX4 (termed SLX4-N), we identify the RNF168 E3 ligase as a critical factor for mitomycin C (MMC)-induced SLX4 foci formation. RNF168 and GFP-SLX4-N colocalize in MMC-induced ubiquitin foci. Accumulation of SLX4-N at psoralen-laser ICL tracks or of endogenous SLX4 at Digoxigenin-psoralen/UVA ICL is dependent on RNF168. Finally, we find that RNF168 is epistatic with SLX4 in promoting MMC tolerance. We conclude that RNF168 is a critical component of the signal transduction that recruits SLX4 to ICL damage.

INTRODUCTION

Fanconi anemia (FA) is a rare hereditary disorder characterized by physical abnormalities, progressive hypoplastic anemia, and development of leukemia and solid tumors (Auerbach, 2009). Cells from FA patients display hypersensitivity to agents that generate DNA interstrand crosslinks (ICLs) such as cancer therapeutic drugs (e.g., mitomycin C [MMC] and cisplatin) or endogenous metabolites (i.e., formaldehyde) (Duxin and Walter, 2015). FA is caused by mutations in any 1 of 22 FA genes that together function in an ICL repair pathway (Ceccaldi et al., 2016). The ICL repair pathway and FA pathogenesis have been extensively studied, revealing an intricate DNA repair and signaling network (Clauson et al., 2013). The presence of ICLs in S phase stalls converging replication forks from two directions, leading to the recognition of the ICL and removal of the Cdc45-MCM-GINS (CMG) helicase complex from the replisome. Mechanistically, this process is achieved by CMG poly-

ubiquitination due to the TRAIP E3 ligase and subsequent unloading by the VCP/p97 ATPase complex (Wu et al., 2019). Following the unloading of CMG, remodeling/reversal of the replication fork probably occurs by the actions of RAD51 and fork remodeling helicases to prevent degradation of the stalled fork (Amunugama et al., 2018). The ICL-induced initial signaling/repair process also involves the FANCM translocase complex, which loads the FA core complex onto chromatin (Kim et al., 2008), mediates the traverse of replicative polymerase across the ICL (Huang et al., 2019), and induces RPA foci formation, enabling efficient ATR kinase activation (Huang et al., 2010; Schwab et al., 2010; Tomida et al., 2013). Loading of the FA core complex is accelerated by local chromosomal polyubiquitination mediated by RNF8 E3 ligase and recognition by the UBZ4 ubiquitin binding domain of FAAP20 protein within the core complex (Yan et al., 2012). It also has been reported that ICLs are recognized by UHRF1 (Liang et al., 2015; Tian et al., 2015) and UHRF2 (Motnenko et al., 2018) proteins.

CellPress
OPEN ACCESS

Cell Reports
Article
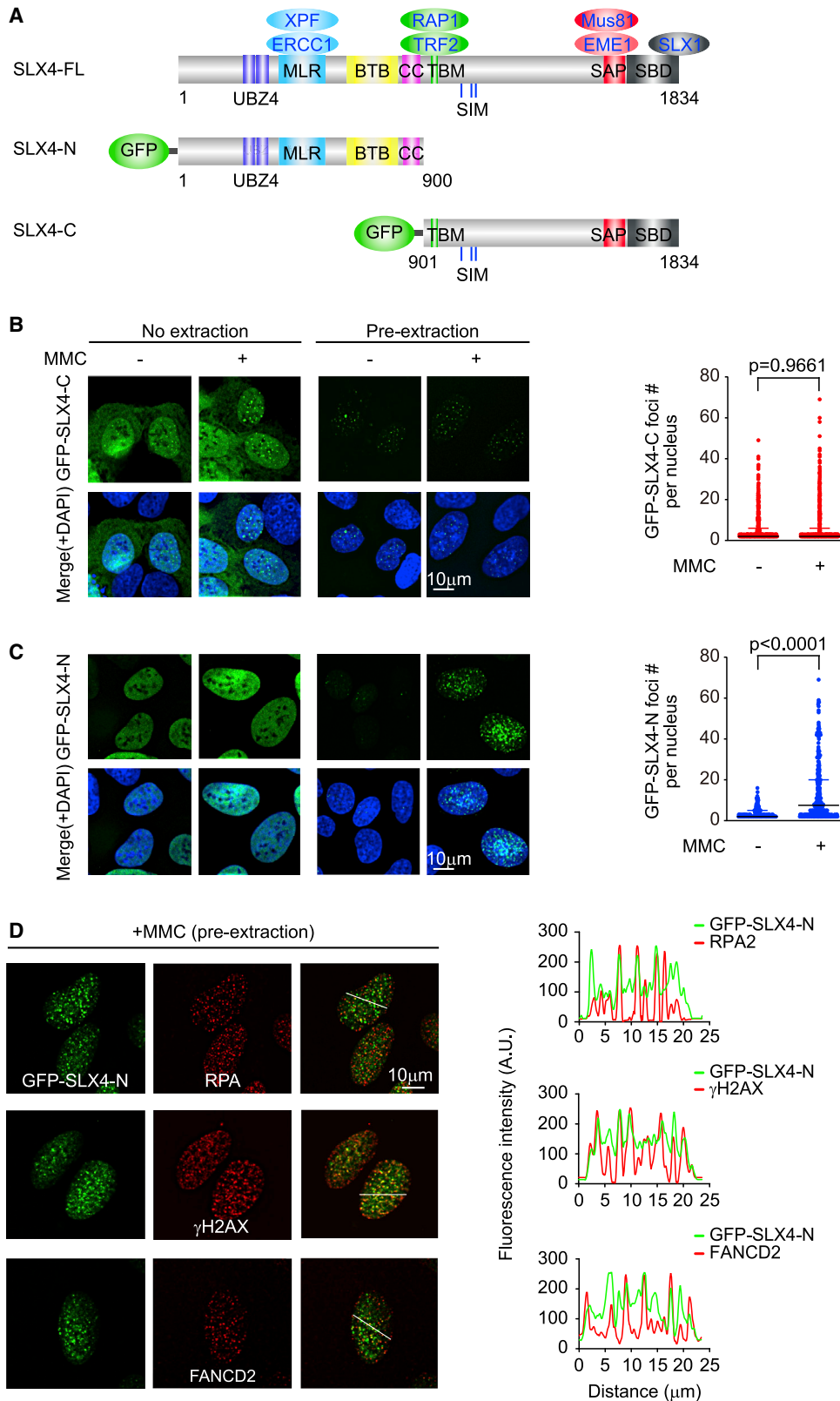
(legend on next page)

Cell Reports
Article

A subsequent step in the ICL repair/FA pathway involves the ATR-mediated phosphorylation of FANCI, leading to structural changes of the FANCD2-FANCI (D2-I) heterodimer complex that allow monoubiquitination of the D2-I complex by the FANCL E3 ligase subunit within the core complex (Ishiai et al., 2008; Sato et al., 2012; Shigechi et al., 2012). This monoubiquitination is critical for D2-I function during ICL repair and replication stress. Recent studies elucidated a striking structural transition of the D2-I complex upon monoubiquitination, resulting in the clamping of DNA, shedding light on how D2-I orchestrates further repair processes and protects stalled forks from degradation (Alcón et al., 2020; Wang et al., 2020).

The next critical step during ICL repair is the dual incision of the ICL on one strand, at both sides of the ICL, termed unhooking, which is mostly mediated by the SLX4 scaffold protein and its partner nuclease XPF-ERCC4 (Hodskinson et al., 2014; Klein Douwel et al., 2014). SLX4 is a large tumor suppressor protein carrying multiple domains, of which each may act as a critical functional module (Dehé and Gaillard, 2017; Guervilly and Gaillard, 2018). These domains include (from the N terminus to the C terminus) the tandem UBZ4 (Ubiquitin binding zinc finger 4) domains, the MLR (Mus312-ME19 interaction-like) domain, the BTB (broad-complex, tramtrack, and bric à brac) domain, the coiled-coil (CC) domain, the TBM (TRF2-binding motif) domain, three SIMs (SUMO-interacting motifs), the SAP (SAF-A/B, Acinus, and PIAS) domain, and the SBD (SLX1-binding domain) (Figure 1A). Of note, the MLR domain is critical for XPF binding and regulation, whereas the BTB mediates functionally important dimerization of SLX4. Furthermore, the SLX4 complex has a SUMO E3 ligase activity, which regulates genome stability during replication stress (Guervilly et al., 2015). The critical function of SLX4 in ICL repair is illustrated by the fact that biallelic mutations in the SLX4 gene result in FA (FA-P subtype) (Kim et al., 2011; Stoepker et al., 2011). Following ICL unhooking, the DNA synthesis resumes across the remnant of the ICL with translesion polymerases, whereas the remaining DNA double strand break (DSB) in one of the sister strands is repaired by homologous recombination using the other sister as a template.

How SLX4 is regulated during the ICL repair process remains controversial. Although SLX4 recruitment to the DNA damage site is mediated by SUMO-SIM interactions in the context of DSB repair, SLX4 functions at the ICL site by ubiquitin-UBZ4 interactions (Guervilly and Gaillard, 2018; Ouyang et al., 2015). This is clearly established, for instance through the identification of FA patients harboring an in-frame deletion within the UBZ4 domains (Guervilly and Gaillard, 2018; Kim et al., 2011; Stoepker et al., 2011).

It has been reported that monoubiquitinated FANCD2 recruits SLX4 by direct binding by the UBZ4 domain in chicken DT40 cells (Yamamoto et al., 2011). In addition, a chromatin immunoprecipitation (ChIP) analysis of an *in vitro* replication assay with a plasmid carrying a defined ICL in *Xenopus* oocyte extracts revealed reduced SLX4 localization near the ICL following FANCD2 depletion (Klein Douwel et al., 2014). This prevailing view has been, however, challenged (Guervilly and Gaillard, 2018). Lachaud et al. (2014) reported that SLX4 is recruited to laser-induced ICLs in a manner independent of FANCD2 in human cells. Furthermore, the same group and others have also shown that the UBZ4 domains of SLX4 preferentially interact with K63-linked polyubiquitin chains but not with a single ubiquitin moiety *in vitro* (Guervilly and Gaillard, 2018; Kim et al., 2011; Lachaud et al., 2014). Interestingly, the recently revealed structure of monoubiquitinated FANCD2 appears to be incompatible with SLX4 binding to the monoubiquitin by the UBZ4 domains because of steric hinderance. Indeed, purified SLX4 cannot be pulled down by a monoubiquitinated D2-I complex in an *in vitro* protein binding assay (Tan et al., 2020). Finally, it is also unknown which E3 ligase provides the ubiquitinated platform onto which SLX4 is recruited by the UBZ4 domains.

In this study, we identified enzymes involved in the ubiquitination cascade that are essential for SLX4 recruitment. We generated and verified a GFP-tagged truncated SLX4 construct corresponding to the N-terminal half of SLX4, which retains full function for ICL repair. Using stably expressed GFP-SLX4-N and its MMC-induced foci formation as a readout, we carried out a small interfering RNA (siRNA) screen largely focusing on proteins involved in the DNA damage response (DDR). Here, we report the identification and characterization of RNF168 as a critical E3 ligase for SLX4 recruitment during signal transduction initiated by ICLs.

RESULTS

The N-terminal half of the SLX4 protein can form ICL-induced foci in a manner dependent on ubiquitin binding

The recruitment of many DNA repair proteins at sites of DNA damage can be followed by the formation of microscopically visible subnuclear foci. However, it has been reported that SLX4 foci are predominantly localized on telomeres in a manner dependent on a TRF2 interaction by the TBM domain (Wan et al., 2013; Wilson et al., 2013). To enumerate DNA-damage-induced SLX4 foci, we stably expressed GFP-tagged full-length human SLX4 in U2OS cells. SLX4 foci already formed under unperturbed conditions, and no significant increase in SLX4 foci
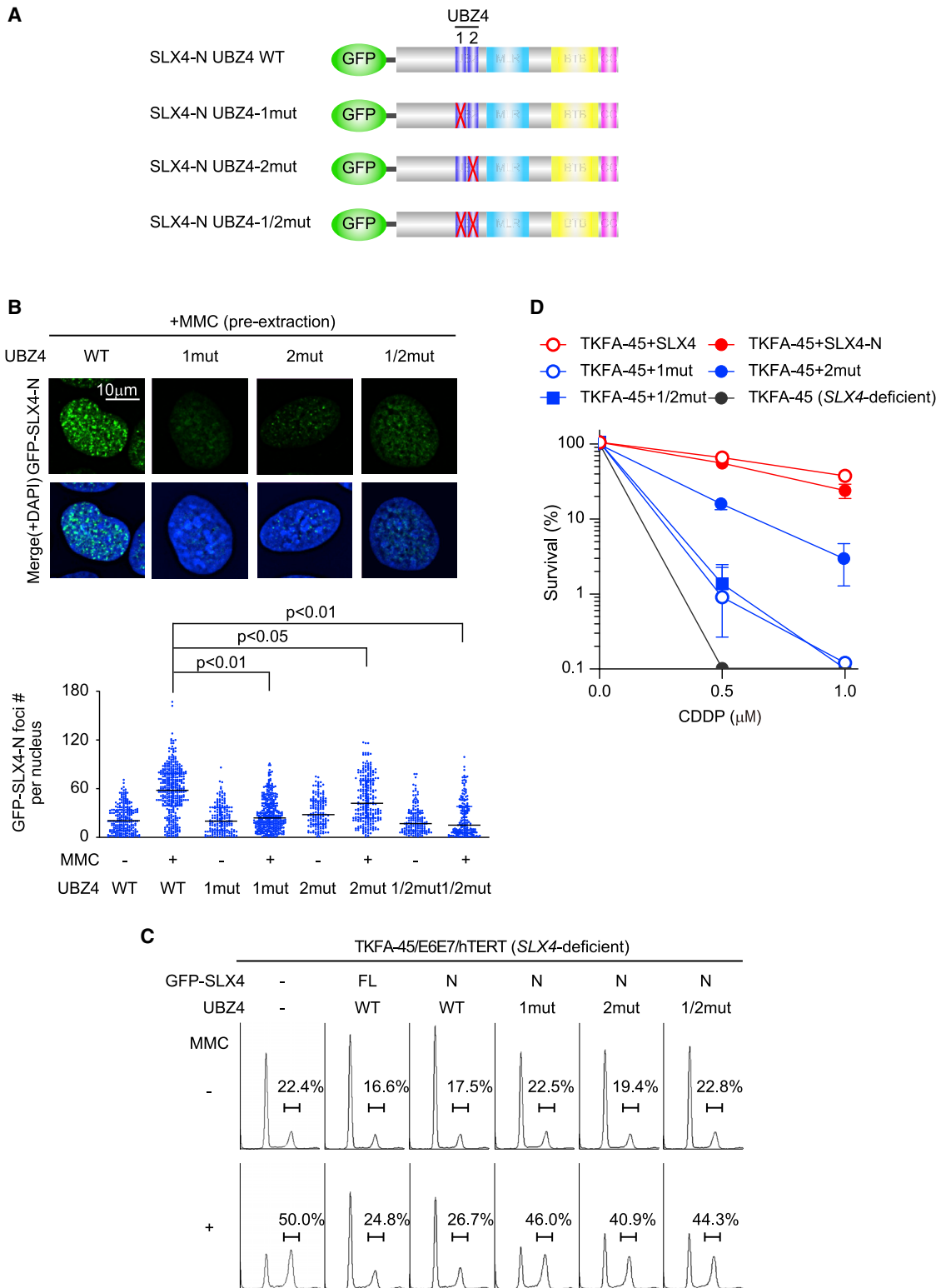
Figure 1. Generation of GFP-SLX4-N to detect ICL-induced foci formation of SLX4

(A) A schematic depiction of full-length (FL), N-terminal (SLX4-N), and C-terminal (SLX4-C) SLX4 protein. The domains and interacting proteins are indicated. UBZ4, Ubiquitin binding zinc finger 4; MLR, Mus312-ME19 interaction-like; BTB, broad-complex, tramtrack, and bric à brac; CC, coiled coil; TBM, TRF2-binding motif; SIM, SUMO-interacting motif; SAP, SAF-A/B, Acinus, and PIAS; SBD, SLX1-binding domain.

(B) Foci formation of GFP-SLX4-C stably expressed in U2OS cells. Cells were treated with or without MMC and fixed with or without pre-extraction. Representative images (left panels) and quantification of the number of foci per nucleus, with median and interquartile range (right), are shown. More than 500 cells were scored. p values were calculated by the Mann-Whitney test.

(C) Foci formation of GFP-SLX4-N stably expressed in U2OS cells. Cells were processed and the results are shown as in (B).

(D) Colocalization of MMC-induced GFP-SLX4-N foci with RPA, γH2AX, or FANCD2 foci. Representative images (left) and fluorescence intensity profiles across nuclear regions indicated by white lines (right) are shown. U2OS cells expressing GFP-SLX4-N were treated with MMC, pre-extracted and fixed, and then stained with the indicated antibodies.

A

SLX4-N UBZ4 WT

SLX4-N UBZ4-1mut

SLX4-N UBZ4-2mut

SLX4-N UBZ4-1/2mut

B

+MMC (pre-extraction)

UBZ4   WT   1mut   2mut   1/2mut

GFP-SLX4-N

Merge(+DAPI)

10μm

p<0.01
p<0.05
p<0.01

MMC   -   +   -   +   -   +   -   +
UBZ4   WT   WT 1mut 1mut 2mut 2mut 1/2mut 1/2mut

D

TKFA-45+SLX4   TKFA-45+SLX4-N
TKFA-45+1mut   TKFA-45+2mut
TKFA-45+1/2mut   TKFA-45 (*SLX4*-deficient)

Survival (%) vs CDDP (μM)

C

TKFA-45/E6E7/hTERT (*SLX4*-deficient)

GFP-SLX4	-	FL	N	N	N	N
UBZ4	-	WT	WT	1mut	2mut	1/2mut
MMC						
-	22.4%	16.6%	17.5%	22.5%	19.4%	22.8%
+	50.0%	24.8%	26.7%	46.0%	40.9%	44.3%

(legend on next page)

京都大学
KYOTO UNIVERSITY

KURENAI 紅
Kyoto University Research Information Repository

Cell Reports
Article

CellPress
OPEN ACCESS

number was observed following MMC treatment (Figure S1A). Treatment of harvested cells with cytoskeleton (CSK) buffer prior to fixation with paraformaldehyde (hereinafter referred to as "pre-extraction") lowers the background by removing loosely bound chromatin proteins and enhances the contrast of nuclear foci (Cramer and Mitchison, 1995). However, even this pre-extraction failed to show a clear increase of SLX4-GFP foci after MMC treatment. We reasoned that DNA-damage-induced foci were probably obscured by the overlapping telomeric foci.

To develop a system with which to measure ICL-induced SLX4 recruitment, we generated N-terminal (amino acid position 1–900) and C-terminal (9001–1834) fragments of the coding sequence of human SLX4 and expressed them as GFP fusions. The N-terminal SLX4 fragment (hereinafter called SLX4-N) contained the UBZ, MLR, and BTB domains, whereas the C-terminal SLX4 fragment carried the TBM, SIMs, and SAP domains and SBD (Figure 1A). When stably expressed in U2OS cells, only GFP-SLX4-N, but not GFP-SLX4-C, was coimmunoprecipitated (coIP) with the ERCC1 protein, which indirectly interacts with the MLR domain of SLX4 by XPF (Figure S1B). We observed that GFP-SLX4-C displayed a punctate localization irrespective of the treatment with MMC or pre-extraction (Figure 1B), reflecting telomere localization (Figure S1C), because SLX4-C contains the TBM domain. In contrast, GFP-SLX4-N foci formation was detected only after pre-extraction, with minimal colocalization at telomeres (Figure S1C), and clearly increased by MMC treatment (Figure 1C) or formaldehyde (Figure S1D). In pre-extracted cells without ICL stimulation, the fluorescent levels of the fusion protein appeared dim because the unbound protein was extracted (Figure 1C). Although the extent of foci formation varied between experiments, perhaps partly because of the difficulty in controlling the rather harsh pre-extraction condition, we consistently observed a significant increase in the foci number following ICL treatments. The MMC-induced GFP-SLX4-N foci were colocalized with several markers of DNA damage and repair, including RPA, γH2AX, and FANCD2, indicating that SLX4-N is recruited to MMC-induced ICLs (Figure 1D). These data indicated that GFP-SLX4-C recognizes telomeres, whereas GFP-SLX4-N detects ICL-induced damages.

Mutations in the tandem UBZ4 domains (encompassing both UBZ4-1 and 4-2) cause deficiency in ICL repair and the FA phenotype in humans and abrogate localization of SLX4 to the damage sites. To confirm the requirement of the UBZ4 domains in the GFP-SLX4-N construct, we generated GFP-SLX4-N variants harboring missense mutations disrupting ubiquitin binding in UBZ4-1, UBZ4-2, or in both (Figure 2A). We observed that, when stably expressed in U2OS cells at nearly equal levels (Figure S2A), the UBZ4-1 mutant markedly impaired foci formation,

whereas the UBZ4-2 mutant only modestly decreased the foci number (Figure 2B). The UBZ4-1/2 double mutations showed similarly decreased SLX4 foci levels to the UBZ4-1 mutant (Figure 2B). These results suggest that the GFP-SLX4-N protein is recruited to DNA damage sites in a manner largely dependent on UBZ4-1-mediated binding of polyubiquitin chain(s) generated at ICL damage sites with some contribution of the UBZ4-2 domain.

Levels of GFP-SLX4-N foci formation are correlated with cellular resistance to ICL damage
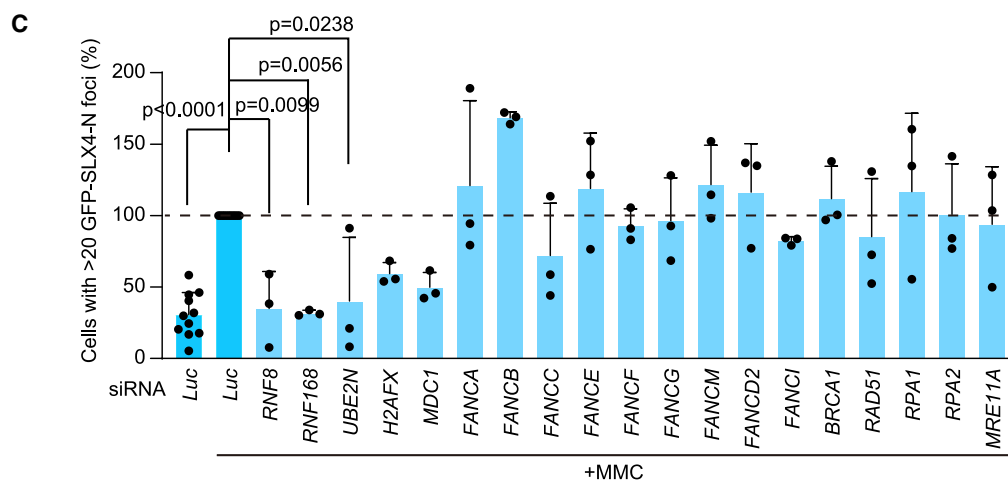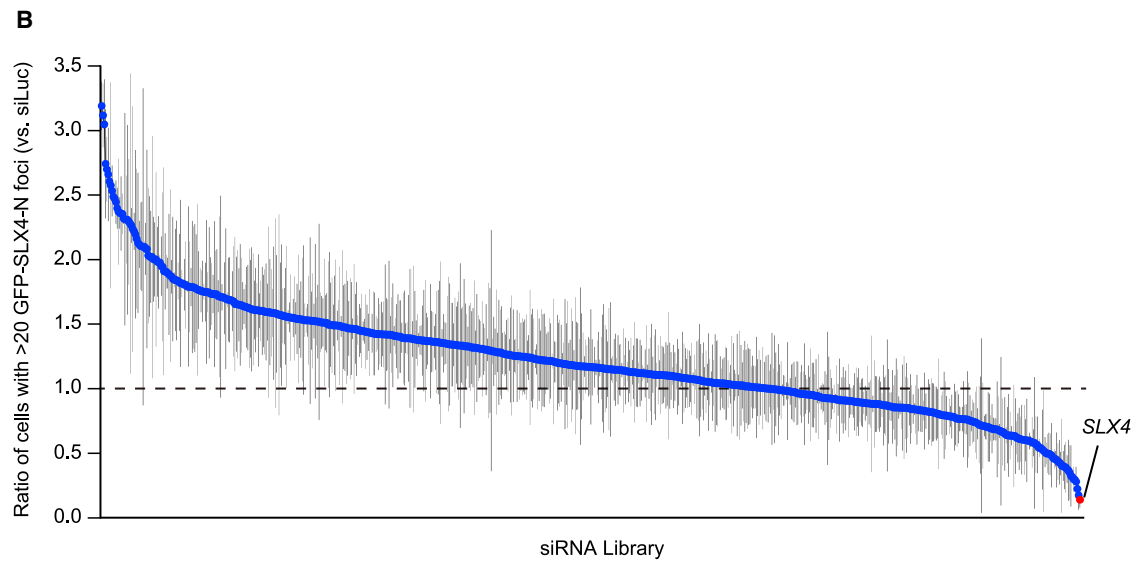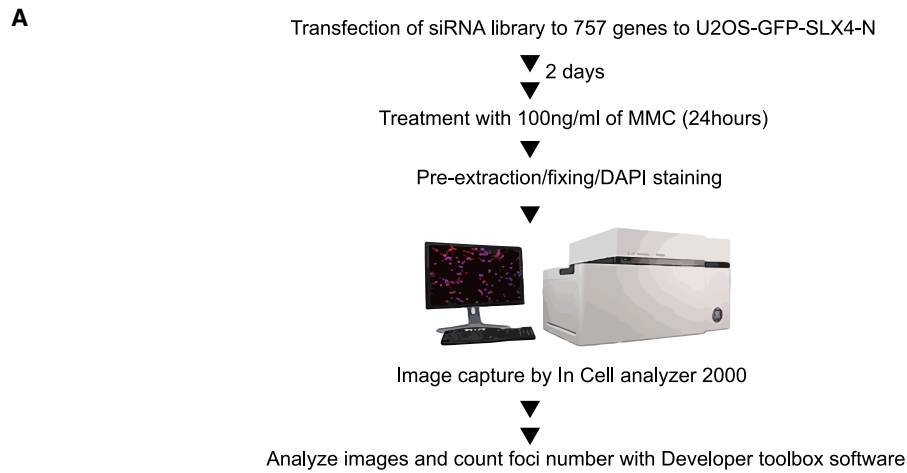
To examine the functionality of GFP-SLX4-N in ICL repair, we expressed full-length wild-type GFP-SLX4, GFP-SLX4-N, and the three GFP-tagged UBZ domain mutants (Figure S2B) in an FA-P fibroblast cell line derived from a Japanese FA-P case, TKFA-45, which was immortalized and transformed by lentiviral introduction of hTERT and papilloma virus E6/E7 (TKFA-45/E6E7/hTERT). TKFA-45 carried homozygous frame-shift mutations of SLX4 (c.343delA and p.S115AfsX11) (Hira et al., 2013). Consistent with the characteristic cell-cycle effects observed in other FA cells, TKFA-45/E6E7/hTERT cells displayed increased levels of G2 arrest after MMC treatment (Figure 2C). Although the expression of both full-length SLX4 and SLX4-N were able to reverse this phenotype, higher levels of G2 arrest were observed in cells expressing SLX4-N disrupted in either UBZ4-1 or UBZ4-2 or both (Figure 2C). We further tested whether expression of these SLX4 variants could alleviate ICL sensitivity in TKFA-45/E6E7/hTERT cells. Expression of full-length or N-terminal SLX4 showed an efficient reversal of the CDDP sensitivity, whereas the UBZ4-1 mutant could only mildly reverse the sensitivity compared to the UBZ4-2 mutant (Figure 2D). Taken together, these results are in line with the prior study that showed N-terminal SLX4 can suppress the ICL sensitivity in SLX4 null cells and all the functional modules necessary for ICL repair are contained in the N-terminal SLX4 half (Hodskinson et al., 2014; Hoogenboom et al., 2019). We concluded that the levels of suppression by the SLX4 variants with regard to ICL sensitivity and ICL-induced G2 arrest correlated well with the levels of foci formation, indicating that foci formation of GFP-SLX4-N can serve as an excellent marker for SLX4 recruitment to sites of ICL DNA damage.

A focused siRNA screen identified a role of RNF168 in SLX4-N foci formation

To identify factors necessary for recruiting SLX4 to ICLs, we carried out an siRNA screen by using a total of 757 siRNA pools (each containing three different siRNAs) targeting genes involved in the DDR, chromatin regulation, or ubiquitination pathways; we

---

Figure 2. SLX4-N forms ICL-induced foci and protects against ICL damage in a manner dependent on the integrity of the UBZ4 domains

(A) A schematic depiction of SLX4-N wild type or with the UBZ4 mutations. WT, wild-type; mut, mutation.

(B) Foci formation of GFP-SLX4-N WT and mutants. U2OS cells expressing the indicated GFP-SLX4-N proteins were stimulated with MMC (100 ng/ml for 24 h) and observed after pre-extraction. Representative images (top) and quantification by an IN Cell Analyzer of GFP-SLX4-N foci (bottom). Median and interquartile range from more than 140 cells scored are shown. p values were calculated by one-way ANOVA with a post hoc test.

(C) MMC-induced cell cycle arrest. TKFA-45/E6E7/hTERT cells and derivatives were treated with MMC (200 nM for 48 h) and analyzed by FACSCalibur flow cytometry following phosphatidylinositol (PI) staining.

(D) Cell survival curves are of parental FA-P TKFA-45/E6E7/hTERT cells and derivatives expressing the indicated mutant SLX4 in the presence of cisplatin (CDDP). Means ± SD of triplicate cultures are shown.

A

Transfection of siRNA library to 757 genes to U2OS-GFP-SLX4-N

▼ 2 days

Treatment with 100ng/ml of MMC (24hours)

▼

Pre-extraction/fixing/DAPI staining

▼

Image capture by In Cell analyzer 2000

▼

Analyze images and count foci number with Developer toolbox software

B

C

(legend on next page)

Cell Reports
Article

CellPress
OPEN ACCESS

used MMC-induced GFP-SLX4-N foci as a readout (Figure 3A; Table S1). Cells stably expressing GFP-SLX4-N were cultured and transfected with the library in 96-well plates, and 48 h later, MMC (100 ng/ml) was added. GFP-foci images were captured by automated cytometry after continuous culturing in the presence of MMC for 24 h. The siRNA screening was repeated three times and siSLX4 served as a positive control. The complete screening results are summarized in Figure 3B and Table S1. High-impact hits included various potentially interesting genes, such as factors that affect ubiquitination and ubiquitin-related modifiers (Table S1). Most interestingly, we noticed that the *RNF168* E3 ligase is the top hit, and other related genes such as *H2FAX*, *MDC1*, *RNF8*, and *UBC13/UBE2N* have an impact on SLX4 foci formation. On the other hand, the canonical FA genes tested such as *FANCD2*, *FANCI*, and *FANCA,* as well as several important DDR genes such as *MRE11A*, *BRCA1*, and *RPA2*, were dispensable (Figure 3C).

The above results regarding the canonical FA proteins are striking given the prevailing view that FANCD2 is required for SLX4 recruitment. To further assess the role of FA proteins in SLX4 recruitment, we expressed GFP-SLX4-N in *FANCA*-deficient and *FANCA*-complemented GM6914 fibroblasts (Figure S3A) and examined GFP-SLX4-N localization before and after MMC treatment. Consistent with the results from the siRNA screening, the absence of *FANCA* did not appreciably affect the GFP-SLX4-N foci formation following MMC treatment (Figure S3B). These results are in line with some, but not all, previous reports, which will be discussed further in the Discussion.

Of note, a prior study identified roles of the ubiquitination cascade mediated by RNF8 during ICL repair and FA pathway activation (Yan et al., 2012). Importantly, the RNF8 and RNF168 can catalyze K63-linked ubiquitin chains (Yan et al., 2012), which fits well with the preferential binding of the SLX4 UBZ4 domains to K-63-linked ubiquitin chains (Guervilly and Gaillard, 2018; Kim et al., 2011; Lachaud et al., 2014). Because UBC13 is an E2 ubiquitin-conjugating enzyme acting with RNF8 to catalyze K63-linked ubiquitin chains, we repeated the experiment with *UBC13* or *RNF8* depletion using an siRNA that was different from those used for the screening (Figure S3C). Indeed, the MMC-induced foci of both GFP-SLX4-N and FK2 were inhibited by siUBC13 or siRNF8 (Figure S3D). These results led us to focus on the role of RNF168 in the ICL-induced SLX4 recruitment.

RNF168 and SLX4 form colocalizing foci in response to ICL-inducing agents

First, we validated our screening data by testing the effect of RNF168 depletion on MMC-induced SLX4 foci formation. U2OS cells expressing GFP-SLX4-N were depleted of RNF168

(again, we used a different siRNA from those used in the screening) and stimulated with MMC or formaldehyde. siRNF168 treatment resulted in a significant decrease in the number of MMC- or formaldehyde-induced GFP-SLX4-N foci per nucleus (Figures 4A and 4B; Figure S3E). The reduction of GFP-SLX4-N foci was observed in S phase nuclei, which were identified based on the anti-PCNA immunofluorescence intensity (Figure S3F). Interestingly, RNF168 depletion also suppressed anti-ubiquitin (FK2) foci induced by MMC (Figures 4A and 4B), which likely reflects polyubiquitination occurring at the ICL sites. It is notable that FK2 foci and GFP-SLX4-N foci colocalized very consistently (Figure 4A, bottom panel). These results support the notion that ICLs can initiate an RNF168-mediated ubiquitin cascade, leading to SLX4 accumulation.

Next, we set out to examine whether RNF168 itself can accumulate in MMC-induced foci. Using a replacement strategy, we transiently transfected U2OS cells with different mCherry-fused RNF168 cDNA constructs that were resistant to an siRNF168 that targets endogenous RNF168 mRNA. We compared the wild type, a RING domain mutant (C16S), or a mutant RNF168 that was unable to interact with its substrate histone H2A (R57D) (Mattiroli et al., 2012). These three RNF168 variants displayed similar levels of foci formation, which were increased following MMC (Figures 4C and 4D), indicating that RNF168 can form foci independent of its E3 ligase activity or its ability to bind H2A. Although a previous report suggested that RNF168 accumulates at DSB sites in a manner dependent on its E3 ligase activity (Panier et al., 2012), our findings here are consistent with several studies that demonstrated that the localization of RNF168 at DSBs depends on the RNF8-mediated ubiquitination of the linker histone H1 (H1.2 and H1x) or the L3MBTL2 (Nowsheen et al., 2018; Thorslund et al., 2015). Interestingly, when wild-type RNF168 is expressed in cells stably expressing GFP-SLX4-N, we found it can induce efficient formation of GFP-SLX4-N foci, and the foci levels increased after MMC treatment (Figures 4C and 4E). The mCherry-RNF168 and GFP-SLX4-N fusion proteins displayed an extensive colocalization as shown in the fluorescence intensity profile (Figure 4C, right graphs). However, the RING domain mutant (C16S) or the mutant incapable of interacting with H2A (R57D) could not induce GFP-SLX4-N foci (Figures 4 and 4E). These results indicate that the catalytic activity of RNF168 leading to H2A ubiquitination is required for SLX4 recruitment to ICL sites.

Forced localization of a LacR-RNF168 fusion at a LacO array recruits SLX4

Previous studies have shown that forced accumulation of a prokaryotic LacR repressor fused with an upstream component in DDR signaling allows damage-induced signal transduction to

---

Figure 3. An siRNA screening identified RNF168 by using MMC-induced GFP-SLX4-N foci as a readout

(A) A schematic depiction of the siRNA screening protocol using U2OS cells expressing GFP-SLX4-N. Cells cultured in 96-well plates were transfected with a mixture containing three different siRNAs and treated 2 days later with MMC for 24 h. Cells were pre-extracted and fixed. Images were captured by an automated cytometer IN Cell Analyzer 2000.

(B) The results of siRNA screening. The experiment was independently repeated three times, and the ratios of cells with more than 20 foci relative to cells transfected with siLuc are shown by the mean (blue dots) with SD (black lines). The data for siSLX4-transfected cells are indicated with a red dot.

(C) The graph depicts the effects of the siRNA targeting 19 indicated genes on GFP-SLX4-N foci. The data from the three independent experiments are indicated by black dots, with mean ± SD. The complete list of siRNA targeted genes (757 in total) and their effects on GFP-SLX4-N foci are provided in Table S1.
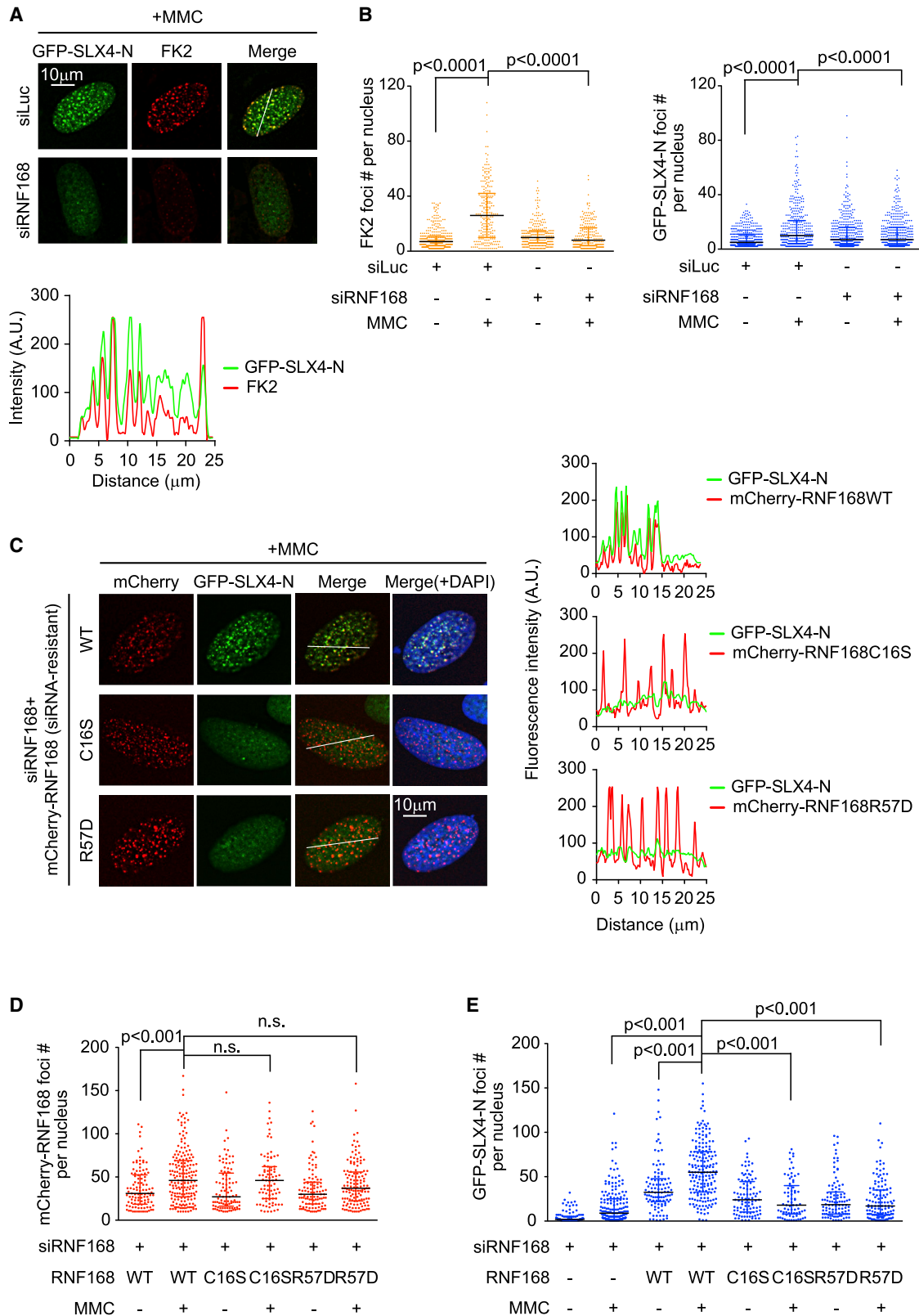
recruit downstream effectors to an integrated 256× array of LacO repeats (Luijsterburg et al., 2017; Soutoglou and Misteli, 2008; Figure 5A). We exploited this system to further corroborate the role of RNF168 in SLX4 recruitment. First, we transiently expressed the mCherry-LacR-RNF168 fusion protein in U2OS 2-6-3 cells that harbor the integrated LacO array and confirmed that the expression induced ubiquitination at the LacO array as detected by anti-FK2 staining, which was colocalized with mCherry foci in 60% of the transfected cells (Figure S4A). However, expression of the control construct (mCherry-LacR-nuclear localization signal [NLS]) induced FK2 dots in ~20% of the transfected cells (Figure S4A). This rather high background ubiquitination at the LacO array may indicate that the LacR expression alone can induce a ubiquitination response, for example, due to mild replication blockage (Beuzer et al., 2014; Kim et al., 2018). Next, we cotransfected GFP-SLX4 constructs together with mCherry-LacR-RNF168 (Figure 5B). The percentage of cells that contained colocalizing GFP-mCherry foci was determined among mCherry-foci positive cells. Expressions of mCherry-LacR-NLS and GFP alone (SLX4 mock) were used as negative controls. We found that chromatin tethering of RNF168 induced high levels of colocalizing foci of mCherry-LacR-RNF168 and GFP-tagged full-length or N-terminal SLX4. Importantly, the levels of colocalizing foci were decreased when GFP-SLX4-N carrying the UBZ4 mutations was expressed (Figure 5B). We also detected endogenous SLX4 accumulated at the LacO array by tethered RNF168 (Figure S4B). U2OS 2-6-3 cells were treated with siSLX4 or siLuc (Figure S4C), and mCherry-LacR-NLS or mCherry-LacR-RNF168 were transiently expressed. Using SLX4 depletion and siLuc control to set the threshold for detection, we observed that a higher percentage of cells displayed anti-SLX4 immunoreactivity at mCherry foci when mCherry-LacR-RNF168 was expressed than those when mCherry-LacR-NLS was expressed (Figures S4B and S4D). These results strongly support the view that ubiquitination at chromatin mediated by RNF168 promotes the accumulation of SLX4.

RNF168 mediates GFP-SLX4-N accumulation at psoralen-laser-induced ICL tracks

It is known that only a fraction (5%–13%) of the adducts induced by MMC are ICLs. In contrast, psoralen-UV-laser-induced DNA damage tracks are mostly composed of ICLs (Muniandy et al., 2010). To verify that an ICL can induce RNF168-mediated SLX4-N recruitment, we set up a system that uses UV-A laser irradiation to generate a track of ICL damage in trimethylpsoralen (TMP)-treated cells. We confirmed that the GFP-SLX4-N accu-

mulated at UV-A laser tracks in TMP-treated (Figure 5C), but not in TMP-untreated (Figure S5A), cells. Furthermore, the accumulation was abrogated by the UBZ4 mutation (Figure 5C) or by siRNF168 (Figure 5D).

RNF168 is required for the recruitment of endogenous full-length SLX4 to ICL sites created by psolaren/UVA

Our data so far used mostly GFP-tagged, exogenously expressed, truncated versions of SLX4. To address whether RNF168 also provides a critical function in the recruitment of endogenous full-length SLX4, we decided to exploit a recently developed system to induce ICLs by digoxigenin (Dig)-TMP and UVA irradiation (Bellani et al., 2018; Figure S5B). This system allowed us to detect SLX4 within a ~40-nm distance to an ICL marked by Dig with the proximity ligation assay (PLA) by using anti-Dig and anti-SLX4 antibodies. We were able to detect increased PLA signals between Dig and SLX4 following UVA in HeLa cells, which were significantly suppressed by both siSLX4 and siRNF168 (Figure S5C). Although the background PLA signal remained between anti-SLX4 and anti-Dig, it was notable that the degree of suppression by the respective siRNAs was not statistically significant (Figure S5C).

RNF168 and SLX4 function in the same pathway during ICL repair

To test whether the loss of RNF168 affects cell survival upon ICL damage, we generated an RNF168 knockout (KO) in an HCT116 colon cancer cell line by using CRISPR-Cas9-mediated genome editing (Figure S6A). We also restored the expression of RNF168 wild type (Figure 6A) or an R57D mutant (Figure 6B) in the KO by a lentiviral constitutive or tet-on inducible expression system, respectively. We observed that the RNF168 KO resulted in the loss of MMC-induced 53BP1 foci formation (Figure S6B) and rendered cells sensitive to cisplatin (Figure 6A), of which the latter was consistent with the reported modest MMC sensitivity of RNF8 knockdown cells (Yan et al., 2012) or cisplatin sensitivity of RNF168 KO mouse embryonic fibroblasts (MEFs) (Zong et al., 2019). Importantly, the ICL sensitivity was rescued following expression of RNF168 WT, but not the R57D mutant, in the *RNF168* KO cells (Figure 6B), indicating that RNF168 and its ubiquitination activity toward H2A are required to protect cells against ICLs. It is also interesting to note that MMC-induced G2 arrest was enhanced in *RNF168* KO compared with wild-type or the complemented KO cells with FLAG-RNF168 (Figure S6C). Furthermore, *RNF168* KO cells displayed significantly reduced recruitment of endogenous SLX4 to ICL created by

---

Figure 4. RNF168 mediates the ubiquitin cascade in response to ICLs and accumulates at ICL-induced foci

(A) RNF168-dependent GFP-SLX4-N foci colocalized with ubiquitin foci. U2OS cells expressing GFP-SLX4-N were transfected with siRNF168, and 48 h later, they were treated with MMC and stained with anti-ubiquitin antibody FK2. Representative images and fluorescence intensity profiles of GFP and FK2 signals across a nuclear region traversed as indicated by white lines are shown.

(B) Quantification of FK2 or SLX4 foci in (A) are shown with medians and interquartile range. More than 200 cells were scored by an IN Cell Analyzer 2000. p values were calculated by one-way ANOVA with a post hoc test.

(C) GFP-SLX4-N foci formation in cells expressing mCherry-RNF168 WT, the RING domain mutant (C16S), or the catalytic mutant (R57D). U2OS cells stably expressing GFP-SLX4-N were depleted of endogenous RNF168 by siRNA and simultaneously transfected with siRNA-resistant mCherry-tagged RNF168 WT or the irrespective mutants. Representative images and fluorescence intensity profiles across a nuclear region traversed as indicted by a white line are shown.

(D and E) Quantification of mCherry-RNF168 foci (D) and GFP-SLX4-N foci (E), with medians and interquartile range, are shown. More than 70 cells were scored by an IN Cell Analyzer 2000. p values were calculated by one-way ANOVA with a post hoc test.

(legend on next page)

Cell Reports
Article

CellPress
OPEN ACCESS
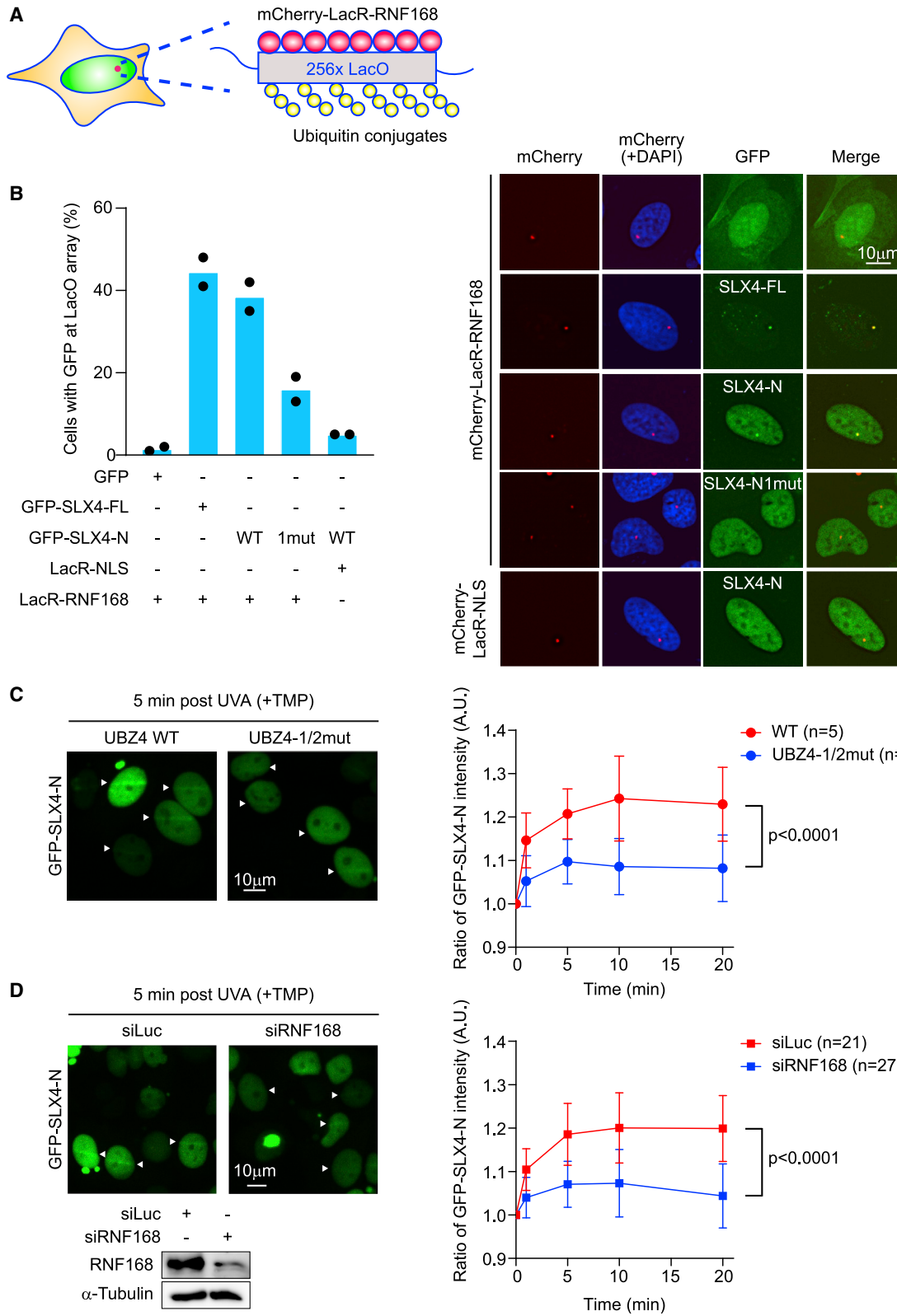
Dig-TMP/UVA, which was reversed by FLAG-RNF168 expression (Figure S6D).

To address epistasis between RNF168 and SLX4 function, we examined whether siRNF168-treated SLX4-deficient TKFA-45/E6E7/hTERT cells showed higher MMC sensitivity than the same cells treated with siLuc. TKFA-45/E6E7/hTERT cells complemented with full-length SLX4 displayed significantly decreased cell survival post-MMC when RNF168 was depleted (Figure 6C). However, the same treatment in TKFA-45/E6E7/hTERT cells did not further affect MMC sensitivity (Figure 6C), consistent with the notion that the role of SLX4 during ICL repair depends on RNF168.

DISCUSSION

Recruitment of SLX4 to DNA damage sites has been difficult to detect because SLX4 displays a complex and damage-independent subcellular localization that is mostly at telomeres (Wan et al., 2013; Wilson et al., 2013). In this study, we bypassed this problem by generating a GFP-tagged N-terminal SLX4 construct (termed GFP-SLX4-N) by deleting the C-terminal half of SLX4. GFP-SLX4-N lacks three SIMs as well as the TBM domain at the middle of the full-length SLX4. These domains are essential for recruiting SLX4 to laser-induced DNA damage (non-ICL) or telomeres, respectively. GFP-SLX4-N expression in an FA-P patient-derived cell line, TKFA-45/E6E7/hTERT, fully reversed the ICL sensitivity, indicating that it contained all the domains required for ICL repair, including the UBZ4 (recruitment), the MLR (XPF binding), and the BTB (dimerization) domains.

Using GFP-SLX4-N, we successfully identified RNF168 and other likely upstream regulators of RNF168, including RNF8, MDC1, and H2AX, as critical factors for GFP-SLX4-N foci formation. Consistently, our work also identified UBC13/UBE2N, which is a known partner E2 enzyme for RNF8, as essential for SLX4 foci formation. RNF168 and GFP-SLX4-N colocalized with ubiquitin foci in cells stimulated with MMC. SLX4 also accumulated at TMP/UVA laser-induced ICL tracks and at a LacO array tethered with LacR-RNF168. We further confirmed the role of RNF168 in the recruitment of endogenous full-length SLX4 by PLA with the Dig-TMP/UVA system. These results established that the ICL-initiated ubiquitination signaling cascade, which involves RNF168, provides a necessary platform to promote ICL repair.

Identification of RNF8-RNF168 ubiquitin ligases as components of an ICL repair pathway is not without precedent. It has

been reported that RNF8 and RNF168 are recruited to the ICL damage created by the psoralen-UV laser in mammalian cells (Yan et al., 2012) and in *Xenopus* egg extracts (Räschle et al., 2015). For example, Yan et al. (2012) found that RNF8 generates K63-linked polyubiquitin chains to activate the FA pathway, recruiting the FA core complex through the UBZ domain of FAAP20, which is one of the core complex components. They speculated that the presence of an ICL triggers ATR activation and that subsequent phosphorylation of MDC1 recruits RNF8, leading to H2A ubiquitination. We envision a similar model, leading to the activation of the ubiquitination signaling. However, it is currently unclear what kind of aberrant DNA structures are recognized by which mechanisms in the context of ICL-initiated signaling.

The siRNA screen also excluded a set of genes that do not play a significant role in SLX4 recruitment, such as canonical FA factors (FANCD2, FANCI, FANCA, and other FA core complex components), or other E3 ligases (RAD18 and BRCA1). We confirmed that FANCA, a component in the FA core E3 ligase critical for ubiquitinating/activating FANCD2, is dispensable for SLX4 recruitment. Previously, Lachaud et al. (2014) used psoralen-UV induced ICLs in mammalian cells, and excluded the role of FANCD2, RAD18, and BRCA1 for SLX4 recruitment. Overall, their results are consistent with our data except for the fact that they also excluded the role of RNF8. It is currently unclear why this discrepancy occurred. On the other hand, our data are in sharp contrast with those of Yamamoto et al. (2011) or Klein Douwel et al. (2014) as discussed in the Introduction. The former study used chicken DT40 cells, whereas the latter group studied a cell-free system using *Xenopus* egg extracts. Different systems or species may differ regarding the dependency of SLX4 on factors required for the recruitment. Although our data suggested FANCD2 and its monoubiquitination are dispensable for SLX4 recruitment in human cells, FANCD2 could still be critical for unhooking activities by SLX4. For example, the DNA clamp activity (Wang et al., 2020) and/or fork protection activity of FANCD2 (Schlacher et al., 2012) may be important for unhooking to occur correctly and efficiently by recruited SLX4. However, it is also notable that Yamamoto et al. (2011) indicated an additive impact on ICL sensitivity by *SLX4* and *FANCC* double knockout.

We observed that the RNF168 KO in HCT116 cells led to mild sensitivity to cisplatin. In line with these data, previous studies reported MMC sensitivity in RNF8 knockdown cells (Yan et al., 2012) or cisplatin sensitivity in MEF cells from


Figure 5. GFP-SLX4-N accumulates at a LacO array when RNF168 is tethered as a LacR fusion or at psoralen-laser-induced ICLs

(A) A schematic depicting the experimental design.

(B) Accumulation of GFP-SLX4 upon tethering of RNF168 at a LacO array. LacR-fused RNF168 or a negative control LacR-NLS (nuclear localization signal) were introduced simultaneously with GFP alone, GFP-SLX4-FL, or GFP-SLX4-N with or without a UBZ4-1 mut into U2OS 2-6-3 cells carrying integrated the LacO array. Cells were then fixed and observed 24 h later without pre-extraction. Representative images and mean percentage of cells with a positive GFP signal at the mCherry-positive LacO array in two independent experiments are shown.

(C) Accumulation of GFP-SLX4-N WT, but not of the UBZ4-1/2 mutant, at ICL tracks induced in MCF7 cells expressing GFP-SLX4-N. Cells were pre-treated with trimethylpsoralen (TMP) and then irradiated by a PALM UVA laser. Representative images and quantification by ImageJ are shown with means ± SD. GFP-SLX4-N accumulation was quantified as the ratio of fluorescence intensity in the irradiated region divided by the background signal within the same nucleus. The p value was calculated comparing WT and the UBZ4 mutant by two-way ANOVA.

(D) Accumulation of GFP-SLX4-N at ICL tracks in a manner dependent on RNF168. MCF7 cells expressing GFP-SLX4-N were treated with siRNA against RNF168 or control siRNA, and the depletion was verified by western blotting. ICL tracks were induced as in (C). Representative images and quantification are shown with means ± SD. The p value was calculated comparing siLuc and siRNF168 conditions by two-way ANOVA.
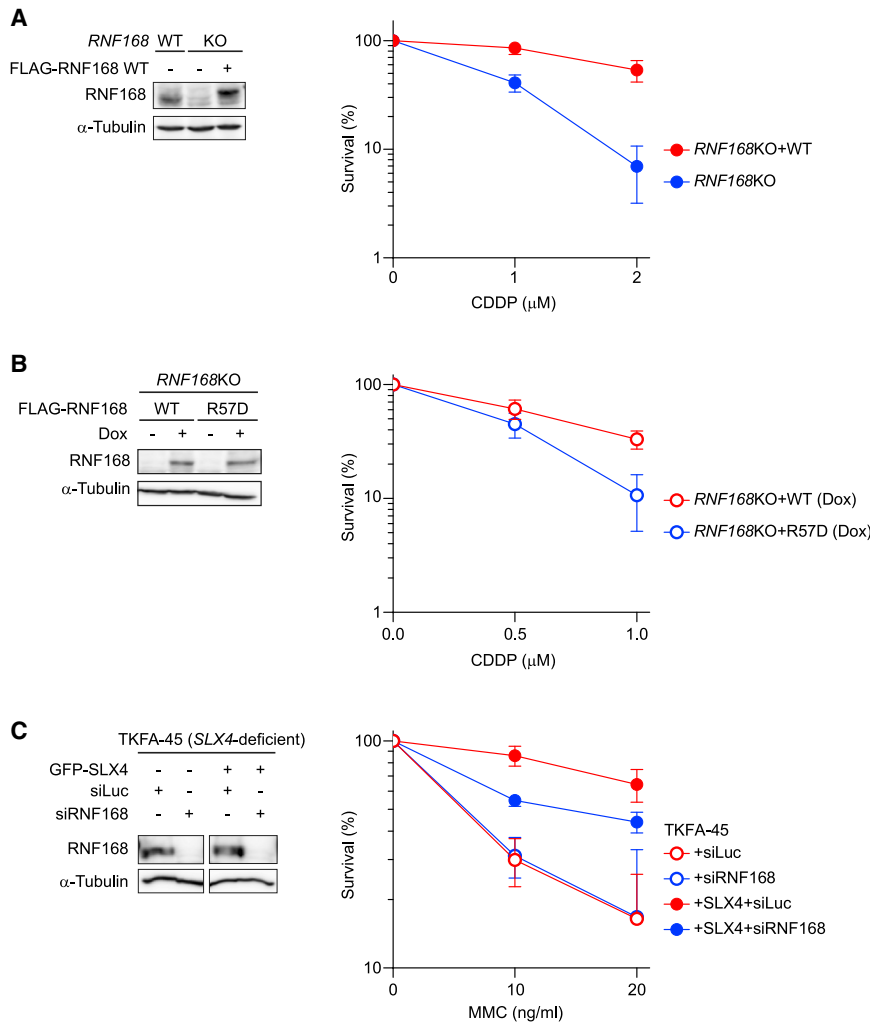
Figure 6. ICL sensitivity of cells lacking expression of RNF168 or SLX4

(A) Shows western blotting and survival assay of RNF168 knockout HCT116 cells complemented or not with FLAG-RNF168. Cells in triplicate cultures were continuously treated with CDDP.

(B) Shows western blotting and survival assay of RNF168 knockout HCT116 cells complemented with FLAG-RNF168 WT or the R57D catalytic mutant. The expression of FLAG-RNF168 was induced by Dox.

(C) Shows western blotting and survival assay of TKFA-45/E6E7/hTERT (FA-P) cells complemented or not with GFP-SLX4-FL and treated with the indicated siRNA. Cells in triplicate cultures were treated with siRNA; 48h later, they were exposed to MMC for 24 h; and then they were re-plated into fresh medium, as described in the STAR Methods. The relative percentages of surviving cells are shown with means ± SD.

(Nakada et al., 2012) by PALB2 targeting (Luijsterburg et al., 2017; Zong et al., 2019); however, this is redundant with BRCA1 function. In the presence of BRCA1, the loss of RNF168 results in only mild or no decrease in RAD51 accumulation levels (Wu et al., 2016; Zong et al., 2019). We suggest that RNF168 may contribute to the ICL repair primarily by SLX4 recruitment in a wild-type setting.

The remaining important question is the identity of the ubiquitinated protein to which the SLX4 UBZ4 domains are binding. H2A is the obvious candidate, and the experiment using the RNF168 R57D mutant suggested that H2A ubiquitination is a prerequisite for SLX4 recruitment. However, a coIP experiment using overexpressed RNF168, SLX4, and FLAG-tagged H2A demonstrated the interaction of ubiquitinated H2A with RNF168 but not with SLX4 (data not shown). Thus, this issue remains obscure and warrants further study.

In conclusion, we identified an RNF168 E3 ligase as a critical factor for SLX4 recruitment during the ICL-initiated signal transduction cascade. The ubiquitination cascade is a hitherto underappreciated branch of the ICL repair pathway that warrants further studies, aiming toward a better understanding of FA (and RIDDLE) pathogenesis and ICL repair mechanisms.

RNF168 KO mice (Zong et al., 2019). The ICL sensitivity in the RNF168 KO appeared to be mild compared to that in the FA cells that was caused by the loss of SLX4, and perhaps this finding is consistent with the lack of an FA phenotype in the RIDDLE syndrome patients (they are described as having radiation sensitivity, dysmorphic features, and learning difficulties) who suffer from RNF168 mutations (Doil et al., 2009; Stewart et al., 2007, 2009). We suggest it is possible that ubiquitin ligase(s) other than RNF8-RNF168 may be involved in SLX4 recruitment and ICL repair in a redundant manner. Our siRNA screen results may be a good starting point to look at this possibility. Alternatively, because RNF168 supports the recruitment of many DNA repair proteins (i.e., 53BP1, BRCA1, RAD18, and PALB2; and now we list here SLX4) to accumulate, the impact of RNF168 loss could be on various aspects of DNA repair pathways such as HR and non-homologous end joining (NHEJ). The mixture of the interfering effects may result in the weaker phenotype. We also note that siRNF168-mediated depletion in SLX4-deficient cells suggested an epistatic relationship. Previous studies established the role of RNF8-RNF168 for RAD51 filament formation

STAR★METHODS

Detailed methods are provided in the online version of this paper and include the following:

- KEY RESOURCES TABLE
- RESOURCE AVAILABILITY
  - ○ Lead contact

Cell Reports
Article

SUPPLEMENTAL INFORMATION

Supplemental information can be found online at https://doi.org/10.1016/j.celrep.2021.109879.

AUTHOR CONTRIBUTIONS

M.T. and Y. Katsuki planned the study with consultation with S.N. and Y. Kim. Y. Katsuki carried out most of the experiments with help from M.A. in automated cytometry, H.v.A. in RNF168 chromatin tethering, W.W. and T.O. in TMP-UV laser experiments, and M.M.S in Dig-TMP/UVA experiments. H.Y. and M.Y. initiated culture of TKFA-45 fibroblasts that was transformed by S.Y.P. and Y. Kim. M.T., Y. Katsuki, M.M.S., and Y. Kim analyzed the data. M.T. and Y. Katsuki wrote the paper.

DECLARATION OF INTERESTS

The authors declare there are no conflicts of interest.

REFERENCES

Adachi, D., Oda, T., Yagasaki, H., Nakasato, K., Taniguchi, T., D'Andrea, A.D., Asano, S., and Yamashita, T. (2002). Heterogeneous activation of the Fanconi anemia pathway by patient-derived FANCA mutants. Hum. Mol. Genet. *11*, 3125–3134.

Alcón, P., Shakeel, S., Chen, Z.A., Rappsilber, J., Patel, K.J., and Passmore, L.A. (2020). FANCD2-FANCI is a clamp stabilized on DNA by monoubiquitination of FANCD2 during DNA repair. Nat. Struct. Mol. Biol. *27*, 240–248.

Amunugama, R., Willcox, S., Wu, R.A., Abdullah, U.B., El-Sagheer, A.H., Brown, T., McHugh, P.J., Griffith, J.D., and Walter, J.C. (2018). Replication Fork Reversal during DNA Interstrand Crosslink Repair Requires CMG Unloading. Cell Rep. *23*, 3419–3428.

Auerbach, A.D. (2009). Fanconi anemia and its diagnosis. Mutat. Res. *668*, 4–10.

Bellani, M.A., Huang, J., Paramasivam, M., Pokharel, D., Gichimu, J., Zhang, J., and Seidman, M.M. (2018). Imaging cellular responses to antigen tagged DNA damage. DNA Repair (Amst.) *71*, 183–189.

Beuzer, P., Quivy, J.-P., and Almouzni, G. (2014). Establishment of a replication fork barrier following induction of DNA binding in mammalian cells. Cell Cycle *13*, 1607–1616.

Ceccaldi, R., Sarangi, P., and D'Andrea, A.D. (2016). The Fanconi anaemia pathway: new players and new functions. Nat. Rev. Mol. Cell Biol. *17*, 337–349.

Clauson, C., Schärer, O.D., and Niedernhofer, L. (2013). Advances in understanding the complex mechanisms of DNA interstrand cross-link repair. Cold Spring Harb. Perspect. Biol. *5*, a012732.

Cramer, L.P., and Mitchison, T.J. (1995). Myosin is involved in postmitotic cell spreading. J. Cell Biol. *131*, 179–189.

Dehé, P.-M., and Gaillard, P.H.L. (2017). Control of structure-specific endonucleases to maintain genome stability. Nat. Rev. Mol. Cell Biol. *18*, 315–330.

Doil, C., Mailand, N., Bekker-Jensen, S., Menard, P., Larsen, D.H., Pepperkok, R., Ellenberg, J., Panier, S., Durocher, D., Bartek, J., et al. (2009). RNF168 binds and amplifies ubiquitin conjugates on damaged chromosomes to allow accumulation of repair proteins. Cell *136*, 435–446.

Duxin, J.P., and Walter, J.C. (2015). What is the DNA repair defect underlying Fanconi anemia? Curr. Opin. Cell Biol. *37*, 49–60.

Guervilly, J.-H., and Gaillard, P.-H.L. (2018). SLX4: multitasking to maintain genome stability. Crit. Rev. Biochem. Mol. Biol. *53*, 475–514.

Guervilly, J.-H., Takedachi, A., Naim, V., Scaglione, S., Chawhan, C., Lovera, Y., Despras, E., Kuraoka, I., Kannouche, P., Rosselli, F., and Gaillard, P.H.L. (2015). The SLX4 complex is a SUMO E3 ligase that impacts on replication stress outcome and genome stability. Mol. Cell *57*, 123–137.

Hira, A., Yabe, H., Yoshida, K., Okuno, Y., Shiraishi, Y., Chiba, K., Tanaka, H., Miyano, S., Nakamura, J., Kojima, S., et al. (2013). Variant ALDH2 is associated with accelerated progression of bone marrow failure in Japanese Fanconi anemia patients. Blood *122*, 3206–3209.

Hodskinson, M.R.G., Silhan, J., Crossan, G.P., Garaycoechea, J.I., Mukherjee, S., Johnson, C.M., Schärer, O.D., and Patel, K.J. (2014). Mouse SLX4 is a tumor suppressor that stimulates the activity of the nuclease XPF-ERCC1 in DNA crosslink repair. Mol. Cell *54*, 472–484.

Hoogenboom, W.S., Boonen, RACM, and Knipscheer, P. (2019). The role of SLX4 and its associated nucleases in DNA interstrand crosslink repair. Nucleic Acids Res *47*, 2377–2388.

Huang, M., Kim, J.M., Shiotani, B., Yang, K., Zou, L., and D'Andrea, A.D. (2010). The FANCM/FAAP24 complex is required for the DNA interstrand crosslink-induced checkpoint response. Mol. Cell *39*, 259–268.

Huang, J., Zhang, J., Bellani, M.A., Pokharel, D., Gichimu, J., James, R.C., Gali, H., Ling, C., Yan, Z., Xu, D., et al. (2019). Remodeling of Interstrand

Crosslink Proximal Replisomes Is Dependent on ATR, FANCM, and FANCD2. Cell Rep. 27, 1794–1808.e5.

Inano, S., Sato, K., Katsuki, Y., Kobayashi, W., Tanaka, H., Nakajima, K., Nakada, S., Miyoshi, H., Knies, K., Takaori-Kondo, A., et al. (2017). RFWD3-Mediated Ubiquitination Promotes Timely Removal of Both RPA and RAD51 from DNA Damage Sites to Facilitate Homologous Recombination. Mol. Cell 66, 622–634.e8.

Ishiai, M., Kitao, H., Smogorzewska, A., Tomida, J., Kinomura, A., Uchida, E., Saberi, A., Kinoshita, E., Kinoshita-Kikuta, E., Koike, T., et al. (2008). FANCI phosphorylation functions as a molecular switch to turn on the Fanconi anemia pathway. Nat. Struct. Mol. Biol. 15, 1138–1146.

Kim, J.M., Kee, Y., Gurtan, A., and D'Andrea, A.D. (2008). Cell cycle-dependent chromatin loading of the Fanconi anemia core complex by FANCM/FAAP24. Blood 111, 5215–5222.

Kim, Y., Lach, F.P., Desetty, R., Hanenberg, H., Auerbach, A.D., and Smogorzewska, A. (2011). Mutations of the SLX4 gene in Fanconi anemia. Nat. Genet. 43, 142–146.

Kim, J., Sturgill, D., Sebastian, R., Khurana, S., Tran, A.D., Edwards, G.B., Kruswick, A., Burkett, S., Hosogane, E.K., Hannon, W.W., et al. (2018). Replication Stress Shapes a Protective Chromatin Environment across Fragile Genomic Regions. Mol. Cell 69, 36–47.e7.

Klein Douwel, D., Boonen, R.A.C.M., Long, D.T., Szypowska, A.A., Räschle, M., Walter, J.C., and Knipscheer, P. (2014). XPF-ERCC1 acts in Unhooking DNA interstrand crosslinks in cooperation with FANCD2 and FANCP/SLX4. Mol. Cell 54, 460–471.

Lachaud, C., Castor, D., Hain, K., Muñoz, I., Wilson, J., MacArtney, T.J., Schindler, D., and Rouse, J. (2014). Distinct functional roles for the two SLX4 ubiquitin-binding UBZ domains mutated in Fanconi anemia. J. Cell Sci. 127, 2811–2817.

Liang, C.-C., Zhan, B., Yoshikawa, Y., Haas, W., Gygi, S.P., and Cohn, M.A. (2015). UHRF1 is a sensor for DNA interstrand crosslinks and recruits FANCD2 to initiate the Fanconi anemia pathway. Cell Rep. 10, 1947–1956.

Luijsterburg, M.S., Typas, D., Caron, M.-C., Wiegant, W.W., van den Heuvel, D., Boonen, R.A., Couturier, A.M., Mullenders, L.H., Masson, J.-Y., and van Attikum, H. (2017). A PALB2-interacting domain in RNF168 couples homologous recombination to DNA break-induced chromatin ubiquitylation. eLife 6, e20922.

Mattiroli, F., Vissers, J.H.A., van Dijk, W.J., Ikpa, P., Citterio, E., Vermeulen, W., Marteijn, J.A., and Sixma, T.K. (2012). RNF168 ubiquitinates K13-15 on H2A/H2AX to drive DNA damage signaling. Cell 150, 1182–1195.

Motnenko, A., Liang, C.-C., Yang, D., Lopez-Martinez, D., Yoshikawa, Y., Zhan, B., Ward, K.E., Tian, J., Haas, W., Spingardi, P., et al. (2018). Identification of UHRF2 as a novel DNA interstrand crosslink sensor protein. PLoS Genet. 14, e1007643.

Muniandy, P.A., Liu, J., Majumdar, A., Liu, S.-T., and Seidman, M.M. (2010). DNA interstrand crosslink repair in mammalian cells: step by step. Crit. Rev. Biochem. Mol. Biol. 45, 23–49.

Nakada, S., Yonamine, R.M., and Matsuo, K. (2012). RNF8 regulates assembly of RAD51 at DNA double-strand breaks in the absence of BRCA1 and 53BP1. Cancer Res. 72, 4974–4983.

Nowsheen, S., Aziz, K., Aziz, A., Deng, M., Qin, B., Luo, K., Jeganathan, K.B., Zhang, H., Liu, T., Yu, J., et al. (2018). L3MBTL2 orchestrates ubiquitin signalling by dictating the sequential recruitment of RNF8 and RNF168 after DNA damage. Nat. Cell Biol. 20, 455–464.

Ouyang, J., Garner, E., Hallet, A., Nguyen, H.D., Rickman, K.A., Gill, G., Smogorzewska, A., and Zou, L. (2015). Noncovalent interactions with SUMO and ubiquitin orchestrate distinct functions of the SLX4 complex in genome maintenance. Mol. Cell 57, 108–122.

Panier, S., Ichijima, Y., Fradet-Turcotte, A., Leung, C.C.Y., Kaustov, L., Arrowsmith, C.H., and Durocher, D. (2012). Tandem protein interaction modules organize the ubiquitin-dependent response to DNA double-strand breaks. Mol. Cell 47, 383–395.

Räschle, M., Smeenk, G., Hansen, R.K., Temu, T., Oka, Y., Hein, M.Y., Nagaraj, N., Long, D.T., Walter, J.C., Hofmann, K., et al. (2015). DNA repair. Proteomics reveals dynamic assembly of repair complexes during bypass of DNA cross-links. Science 348, 1253671.

Sato, K., Toda, K., Ishiai, M., Takata, M., and Kurumizaka, H. (2012). DNA robustly stimulates FANCD2 monoubiquitylation in the complex with FANCI. Nucleic Acids Res. 40, 4553–4561.

Schlacher, K., Wu, H., and Jasin, M. (2012). A distinct replication fork protection pathway connects Fanconi anemia tumor suppressors to RAD51-BRCA1/2. Cancer Cell 22, 106–116.

Schwab, R.A., Blackford, A.N., and Niedzwiedz, W. (2010). ATR activation and replication fork restart are defective in FANCM-deficient cells. EMBO J. 29, 806–818.

Shigechi, T., Tomida, J., Sato, K., Kobayashi, M., Eykelenboom, J.K., Pessina, F., Zhang, Y., Uchida, E., Ishiai, M., Lowndes, N.F., et al. (2012). ATR-ATRIP kinase complex triggers activation of the Fanconi anemia DNA repair pathway. Cancer Res. 72, 1149–1156.

Soutoglou, E., and Misteli, T. (2008). Activation of the cellular DNA damage response in the absence of DNA lesions. Science 320, 1507–1510.

Stewart, G.S., Stankovic, T., Byrd, P.J., Wechsler, T., Miller, E.S., Huissoon, A., Drayson, M.T., West, S.C., Elledge, S.J., and Taylor, A.M.R. (2007). RIDDLE immunodeficiency syndrome is linked to defects in 53BP1-mediated DNA damage signaling. Proc. Natl. Acad. Sci. USA 104, 16910–16915.

Stewart, G.S., Panier, S., Townsend, K., Al-Hakim, A.K., Kolas, N.K., Miller, E.S., Nakada, S., Ylanko, J., Olivarius, S., Mendez, M., et al. (2009). The RIDDLE syndrome protein mediates a ubiquitin-dependent signaling cascade at sites of DNA damage. Cell 136, 420–434.

Stoepker, C., Hain, K., Schuster, B., Hilhorst-Hofstee, Y., Rooimans, M.A., Steltenpool, J., Oostra, A.B., Eirich, K., Korthof, E.T., Nieuwint, A.W.M., et al. (2011). SLX4, a coordinator of structure-specific endonucleases, is mutated in a new Fanconi anemia subtype. Nat. Genet. 43, 138–141.

Tan, W., van Twest, S., Leis, A., Bythell-Douglas, R., Murphy, V.J., Sharp, M., Parker, M.W., Crismani, W., and Deans, A.J. (2020). Monoubiquitination by the human Fanconi anemia core complex clamps FANCI:FANCD2 on DNA in filamentous arrays. eLife 9, 240.

Thorslund, T., Ripplinger, A., Hoffmann, S., Wild, T., Uckelmann, M., Villumsen, B., Narita, T., Sixma, T.K., Choudhary, C., Bekker-Jensen, S., and Mailand, N. (2015). Histone H1 couples initiation and amplification of ubiquitin signalling after DNA damage. Nature 527, 389–393.

Tian, Y., Paramasivam, M., Ghosal, G., Chen, D., Shen, X., Huang, Y., Akhter, S., Legerski, R., Chen, J., Seidman, M.M., et al. (2015). UHRF1 contributes to DNA damage repair as a lesion recognition factor and nuclease scaffold. Cell Rep. 10, 1957–1966.

Tomida, J., Itaya, A., Shigechi, T., Unno, J., Uchida, E., Ikura, M., Masuda, Y., Matsuda, S., Adachi, J., Kobayashi, M., et al. (2013). A novel interplay between the Fanconi anemia core complex and ATR-ATRIP kinase during DNA crosslink repair. Nucleic Acids Res. 41, 6930–6941.

Unno, J., Itaya, A., Taoka, M., Sato, K., Tomida, J., Sakai, W., Sugasawa, K., Ishiai, M., Ikura, T., Isobe, T., et al. (2014). FANCD2 binds CtIP and regulates DNA-end resection during DNA interstrand crosslink repair. Cell Rep. 7, 1039–1047.

Wan, B., Yin, J., Horvath, K., Sarkar, J., Chen, Y., Wu, J., Wan, K., Lu, J., Gu, P., Yu, E.Y., et al. (2013). SLX4 assembles a telomere maintenance toolkit by bridging multiple endonucleases with telomeres. Cell Rep. 4, 861–869.

Wang, R., Wang, S., Dhar, A., Peralta, C., and Pavletich, N.P. (2020). DNA clamp function of the monoubiquitinated Fanconi anaemia ID complex. Nature 580, 278–282.

Wilson, J.S.J., Tejera, A.M., Castor, D., Toth, R., Blasco, M.A., and Rouse, J. (2013). Localization-dependent and -independent roles of SLX4 in regulating telomeres. Cell Rep. 4, 853–860.

Wu, W., Togashi, Y., Johmura, Y., Miyoshi, Y., Nobuoka, S., Nakanishi, M., and Ohta, T. (2016). HP1 regulates the localization of FANCJ at sites of DNA double-strand breaks. Cancer Sci. 107, 1406–1415.

Cell Reports
Article

Wu, R.A., Semlow, D.R., Kamimae-Lanning, A.N., Kochenova, O.V., Chistol, G., Hodskinson, M.R., Amunugama, R., Sparks, J.L., Wang, M., Deng, L., et al. (2019). TRAIP is a master regulator of DNA interstrand crosslink repair. Nature 567, 267–272.

Yamamoto, K.N., Kobayashi, S., Tsuda, M., Kurumizaka, H., Takata, M., Kono, K., Jiricny, J., Takeda, S., and Hirota, K. (2011). Involvement of SLX4 in interstrand cross-link repair is regulated by the Fanconi anemia pathway. Proc. Natl. Acad. Sci. USA 108, 6492–6496.

Yan, Z., Guo, R., Paramasivam, M., Shen, W., Ling, C., Fox, D., 3rd, Wang, Y., Oostra, A.B., Kuehl, J., Lee, D.-Y., et al. (2012). A ubiquitin-binding protein, FAAP20, links RNF8-mediated ubiquitination to the Fanconi anemia DNA repair network. Mol. Cell 47, 61–75.

Zhang, J., Bellani, M.A., James, R.C., Pokharel, D., Zhang, Y., Reynolds, J.J., McNee, G.S., Jackson, A.P., Stewart, G.S., and Seidman, M.M. (2020). DONSON and FANCM associate with different replisomes distinguished by replication timing and chromatin domain. Nat. Commun. 11, 3951.

Zong, D., Adam, S., Wang, Y., Sasanuma, H., Callén, E., Murga, M., Day, A., Kruhlak, M.J., Wong, N., Munro, M., et al. (2019). BRCA1 Haploinsufficiency Is Masked by RNF168-Mediated Chromatin Ubiquitylation. Mol. Cell 73, 1267–1281.e7.

STAR★METHODS

KEY RESOURCES TABLE

REAGENT or RESOURCE	SOURCE	IDENTIFIER
Antibodies		
Mouse monoclonal anti-GFP	MBL	Cat# M048-3; RRID:AB_591823
Rabbit polyclonal anti-RNF168	Millipore	Cat# ABE367; RRID:AB_11212809
Mouse monoclonal anti-phospho-histone H2A.X (Ser139)	Upstate	Cat# 05-636; RRID:AB_309864
Mouse monoclonal anti-RPA2	Abcam	Cat# ab2175; RRID:AB_302873
Rabbit polyclonal anti-FANCD2	Novus	Cat# NB100-182; RRID:AB_10002867
Rabbit polyclonal anti-FANCA	Bethyl	Cat# A301-980A; RRID:AB_1547945
Mouse monoclonal anti-α-Tubulin	Sigma-Aldrich	Cat# T5168; RRID:AB_477579
Mouse monoclonal anti-UBC13	Santa Cruz	Cat# sc-376470; RRID:AB_11150503
Mouse monoclonal anti-Multi ubiquitin (FK2)	Nippon Biotest Laboratories	Cat# 302-06751; RRID:AB_2893311
Rabbit polyclonal anti-SLX4	Bethyl	Cat# A302-270A; RRID:AB_1850156
Mouse monoclonal anti-53BP1	BD	Cat# 612523; RRID:AB_399824
Mouse monoclonal anti-RNF8	Santa Cruz	Cat# sc-271462; RRID:AB_10648902
Mouse monoclonal anti-PCNA	Santa Cruz	Cat# sc-56; RRID:AB_628110
Mouse monoclonal anti-Digoxigenin (Dig)	Abcam	Cat# ab420; RRID:AB_304362
Mouse monoclonal anti-TRF2	Millipore	Cat# 05-521; RRID:AB_2303145
Rat anti-GFP, magnetic beads	MBL	Cat# D153-11; RRID:AB_2893312
Goat anti-mouse IgG(H+L), Alexa Fluor 594	Invitrogen	Cat# A11032; RRID:AB_2534091
Goat anti-rabbit IgG(H+L), Alexa Fluor 594	Invitrogen	Cat# A11037; RRID:AB_2534095
Sheep anti-mouse IgG, HRP-linked F(ab')$_2$ fragment	Cytiva	Cat# NA9310-1ML; RRID:AB_772193
Donkey anti-rabbit IgG, HRP-linked F(ab')$_2$ fragment	Cytiva	Cat# NA9340-1ML; RRID:AB_772191
Bacterial and virus strains		
Bacteria: DH5α	TOYOBO	Cat# DNA-903
Bacteria: Stbl3	Invitrogen	Cat# C7373-03
Bacteria: *ccdB* Survival 2T1	Invitrogen	Cat# CA10460
Chemicals, peptides, and recombinant proteins		
Mitomycin C	Kyowa Kirin	N/A
Mitomycin C	Nacalai tesque	Cat# 20898-21
Cisplatin (CDDP)	Nippon Kayaku	N/A
Formaldehyde	Polysciences	Cat# 18814-10
Trioxsalen (trimethylpsoralen)	Sigma-Aldrich	Cat# T6137
PhosSTOP, phosphatase inhibitor	Roche	Cat# 4906837001
cOmplete, EDTA-free Protease Inhibitor Cocktail	Roche	Cat# 4693132001
Digoxigenin-trimethylpsoralen (Dig-TMP)	Bellani et al., 2018	N/A
Critical commercial assays		
Gateway LR Clonase II Enzyme mix	Invitrogen	Cat# 11791-020
In-Fusion HD Cloning Kit	Clontech	Cat# 639648
Duolink *In Situ* PLA Probe Anti-Mouse MINUS	Sigma-Aldrich	Cat# DUO92004; RRID:AB_2713942
Duolink *In Situ* PLA Probe Anti-Rabbit PLUS	Sigma-Aldrich	Cat# DUO92002; RRID:AB_2810940
Duolink *In Situ* Detection Reagents Orange	Sigma-Aldrich	Cat# DUO92007
Duolink *In Situ* Wash Buffers, Fluorescence	Sigma-Aldrich	Cat# DUO82049

(Continued on next page)

Cell Reports
Article

Continued

REAGENT or RESOURCE	SOURCE	IDENTIFIER
Deposited data		
Raw data deposited in Mendeley Data repository	This paper	http://data.mendeley.com/v1/datasets/bwdj9tvssg/draft?a=52139563-7de1-4a10-a1c6-f0878ac0fab5
Experimental models: Cell lines		
Human: TKFA-45/E6E7/hTERT (EHT) cells	This paper	N/A
Human: TKFA-45/EHT-tet-inducible GFP-SLX4-FL	This paper	N/A
Human: TKFA-45/EHT tet-inducible GFP-SLX4-N	This paper	N/A
Human: TKFA-45/EHT-tet-inducible GFP-SLX4-N (UBZ4-1mut)	This paper	N/A
Human: TKFA-45/EHT-tet-inducible GFP-SLX4-N (UBZ4-2mut)	This paper	N/A
Human: TKFA-45/EHT-tet-inducible GFP-SLX4-N (UBZ4-1/2mut)	This paper	N/A
Human: HCT116 cells RNF168KO	This paper	N/A
Human: HCT116 cells RNF168KO-FLAG-RNF168 (WT) complemented	This paper	N/A
Human: HCT116 cells RNF168KO-tet-inducible FLAG-RNF168 (WT)	This paper	N/A
Human: HCT116 cells RNF168KO-tet-inducible FLAG-RNF168 (R57D)	This paper	N/A
Human: MCF7 cells with GFP-SLX4-N	This paper	N/A
Human: MCF7 cells with GFP-SLX4-N (UBZ4-1mut)	This paper	N/A
Human: U2OS cells	Unno et al., 2014	N/A
Human: U2OS 2-6-3 cells	Soutoglou and Misteli, 2008	N/A
Human: U2OS cells with GFP-SLX4-FL	This paper	N/A
Human: U2OS cells with GFP-SLX4-N	This paper	N/A
Human: U2OS cells with GFP-SLX4-N (UBZ4-1mut)	This paper	N/A
Human: U2OS cells with GFP-SLX4-N (UBZ4-2mut)	This paper	N/A
Human: U2OS cells with GFP-SLX4-N (UBZ4-1/2mut)	This paper	N/A
Human: GM6914 cells	Adachi et al., 2002	N/A
Human: GM6914 cells complemented with FANCA	Tomida et al., 2013	N/A
Oligonucleotides		
siRNA targeting sequence: RNF168#1: GACACUUUCUCCACAGAUATT	This paper	N/A
siRNA targeting sequence: SLX4#2: GAGAAGAACCCUAAUGAAATT	This paper	N/A
siRNA targeting sequence: UBC13: AACCAGGUCUUUAGAAUAUTT	Inano et al., 2017	N/A
siRNA targeting sequence: RNF8: GGAGAUAGCCCAAGGAGAATT	Nakada et al., 2012	N/A
Primers for SLX4 mutagenesis and generation of RNF168KO cells, see Table S2	This paper	N/A
Recombinant DNA		
CSII-CMV-GFP-SLX4-FL-IRES-Bsd	This paper	N/A
CSII-CMV-GFP-SLX4-N-IRES-Bsd	This paper	N/A
CSII-CMV-GFP-SLX4-C-IRES-Bsd	This paper	N/A

(*Continued on next page*)

Continued

REAGENT or RESOURCE	SOURCE	IDENTIFIER
CSII-CMV-GFP-SLX4-N(UBZ4-1mut)-IRES-Bsd	This paper	N/A
CSII-CMV-GFP-SLX4-N(UBZ4-2mut)-IRES-Bsd	This paper	N/A
CSII-CMV-GFP-SLX4-N(UBZ4-1/2mut)-IRES-Bsd	This paper	N/A
CSIV-TRE-GFP-SLX4-FL-UbC-puro	This paper	N/A
CSIV-TRE-GFP-SLX4-N-UbC-puro	This paper	N/A
CSIV-TRE-GFP-SLX4-N (UBZ4-1mut)-UbC-puro	This paper	N/A
CSIV-TRE-GFP-SLX4-N (UBZ4-2mut)-UbC-puro	This paper	N/A
CSIV-TRE-GFP-SLX4-N (UBZ4-1/2mut)-UbC-puro	This paper	N/A
pcDNA3.1-GFP	This paper	N/A
pcDNA3.1-GFP-SLX4-FL	This paper	N/A
pcDNA3.1-GFP-SLX4-N	This paper	N/A
pcDNA3.1-GFP-SLX4-N (UBZ4-1mut)	This paper	N/A
CSII-CMV-FLAG-RNF168 (WT)-IRES-Bsd	This paper	N/A
CSIV-TRE-FLAG-RNF168 (WT)-UbC-puro	This paper	N/A
CSIV-TRE-FLAG-RNF168 (R57D)-UbC-puro	This paper	N/A
pcDNA3.1-mCherry-RNF168(WT) siRNA-resistant	This paper	N/A
pcDNA3.1-mCherry-RNF168 (C16S) siRNA-resistant	This paper	N/A
pcDNA3.1-mCherry-RNF168 (R57D) siRNA-resistant	This paper	N/A
pENTR-GFP-SLX4	This paper	N/A
pENTR-RNF168 siRNA-resistant	This paper	N/A
Software and algorithms		
IN Cell Developer Toolbox	Cytiva	https://www.gelifesciences.co.kr/wp-content/uploads/2016/08/IN-Cell-Developer-Toolbox-v1.9.pdf ; RRID:SCR_015790
BZ II Analyzer	Keyence	https://www.keyence.com/
ImageJ	NIH	https://imagej.net/; RRID:SCR_003070
GraphPad Prism (ver.5 and 8)	GraphPad	https://www.graphpad.com; RRID:SCR_002798
BD CellQuest Pro	BD	https://www.cnbc.pt/pdf/BD_CellQuest_Analysis_Tutorial.pdf ; RRID:SCR_014489
BD FACSDiva	BD	https://www.bdbiosciences.com/ja-jp/products/software/instrument-software/bd-facsdiva-software; RRID:SCR_001456

RESOURCE AVAILABILITY

Lead contact

Further information and requests for resources and reagents should be directed to and will be fulfilled by the lead contact, Dr. Minoru Takata (takata.minoru.8s@kyoto-u.ac.jp).

Materials availability

This study did not generate new unique reagents.

Data and code availability

All data reported in this paper will be shared by the lead contact upon request.

This paper does not report original code.

Any additional information required to reanalyze the data reported in this paper is available from the lead contact upon request.

Cell Reports
Article

CellPress
OPEN ACCESS

EXPERIMENTAL MODEL AND SUBJECT DETAILS

Cell culture

All cell lines were maintained in a humidified incubator at 37°C, 5% CO$_2$. U2OS cells, and U2OS 2-6-3 cells containing a LacO array were grown in DMEM (high glucose) with 10% fetal bovine serum (FBS). MCF7 cells were maintained in MEM with 10% FBS. HCT116 cells were maintained in McCoy's 5A (Invitrogen) supplemented with 10% FBS and 2 mM L-Glutamine (L-Glu). *FANCA*-deficient (GM6914) and *FANCA*-complemented (GM6914 complemented with *FANCA*) fibroblasts were obtained from Dr. Takayuki Yamashita (Gunma university), and were maintained in DMEM with 10% FBS. The Japanese FA-P patient fibroblasts TKFA-45 were cultured from a biopsied skin sample and immortalized and transformed with hTERT, HPV E6 and E7 proteins, as previously described (Kim et al., 2011), and were grown in RPMI1640 with 20% FBS. All media except for McCoy's 5A and L-Glu were obtained from nacalai tesque. FBS was purchased from GIBCO or Sigma-Aldrich.

METHOD DETAILS

Plasmid constructs

Human *SLX4* (a gift from Dr. John Rouse, University of Dundee) and *RNF168* (Luijsterburg et al., 2017) cDNAs were amplified and subcloned into pENTR entry vector (Invitrogen), and transferred to a mammalian expression vector (pcDNA3.1, Thermo Fisher) or lentiviral vectors CSII-CMV-MCS-IRES2-Bsd (provided by Dr. Hiroyuki Miyoshi) modified to harbor a Gateway cassette RfA sequence, or CSIV-TRE-RfA-UbC-puro (provided by Drs. Hiroyuki Miyoshi and Makoto Nakanishi) by Gateway LR Clonase II (Invitrogen). siRNA-resistant mCherry-LacR-RNF168 plasmids were previously described (Luijsterburg et al., 2017). Deletions and missense mutations in plasmids were generated by PCR using KOD-FX or KOD-plus-neo polymerases (TOYOBO) and an In-Fusion HD Cloning Kit (Clontech) or Gibson assembly. Mutations generated were confirmed by Sanger sequencing with an ABI PRISM 3130 Genetic Analyzer (Applied Biosystems). Primers used in this study are listed in Table S2.

Antibodies and reagents

The following antibodies were obtained from commercial sources: anti-GFP (MBL, M048-3), anti-RNF168 (Millipore, ABE367), anti-phospho-histone H2AX (Upstate, 05-636), anti-RPA2 (Abcam, ab2175), anti-FANCD2 (Novus, NB100-182), anti-FANCA (Bethyl, A301-980A), anti-α-tubulin (Sigma-Aldrich, T5168), anti-UBC13 (Santa Cruz, sc-376470), anti-RNF8 (Santa Cruz, sc-271462), anti-Multi ubiquitin (FK2)(Nippon Bio-Test Laboratories, 302-06751), anti-SLX4 (Bethyl, A302-270A), anti-53BP1 (BD, 612523), anti-Digoxigenin (Dig) (Abcam, ab420), anti-PCNA (Santa Cruz, sc-56), anti-TRF2 (Millipore, 05-521, kindly provided from Drs. Fuyuki Ishikawa and Tomoichiro Miyoshi). For secondary antibodies, anti-mouse IgG (A11032) or anti-rabbit IgG (A11037), Alexa Fluor 594-conjugated (Molecular Probes), and anti-mouse IgG (NA9310-1ML) or anti-rabbit IgG (NA9340-1ML), HRP-linked F(ab')$_2$ fragment (G.E. Healthcare) were used. Mitomycin C, cisplatin (CDDP), formaldehyde, and trioxsalen (trimethylpsoralen) were purchased from Kyowa Kirin or nacalai tesque, Nippon Kayaku, Polysciences, and Sigma-Aldrich, respectively.

Transfections

For siRNA screening, the Silencer Select Human Genome siRNA Library (96-well, 3 siRNA per pool) was used (Ambion). Individual siRNA duplexes were purchased from Invitrogen or Sigma-Aldrich, and RNA oligo sequences are listed in Table S2. Transfection of siRNA was carried out using Lipofectamine RNAiMAX (Invitrogen) according to the manufacturer's instructions. For co-transfection of plasmids with siRNA, Lipofectamine 3000 (Invitrogen) was used.

Fluorescence imaging of subnuclear foci

Cells were grown in 96-well black/clear bottom microplates (B.D., 351329) or on a coverslip (Matsunami) in 6-well plates (Greiner). After treatment with DNA damaging agents, cells were washed with PBS and pre-extracted with CSK buffer (10mM Pipes, pH 6.8, 300 mM sucrose, 100 mM NaCl, 3 mM MgCl$_2$) containing 0.5% Triton X-100 for 5 min on ice. Then cells were fixed with 3% paraformaldehyde/2% sucrose solution for 15 min and permeabilized with 0.2% Triton X-100/PBS for 5 min. For PCNA staining, cells were additionally treated with 100% ice-cold methanol for 15 min at −20°C. After blocking with 2% BSA/PBS, staining with primary antibodies diluted in 2% BSA/PBS was performed for 1 h at room temperature (RT), followed by incubating with secondary antibodies with DAPI (4′, 6-diamidino-2-phenylindole) for 1 h at RT. Images were captured by automated cytometry using an IN Cell Analyzer 2000 equipped with an ASAC 60X 0.7 NA lens (G.E. Healthcare) and processed using Developer Toolbox software. Alternatively, cells were observed by a BZ-9000 fluorescence microscope (Keyence) with a Plan Apo l 40X/NA 0.95 objective lens (Nikon).

Cell survival assay

To measure cell survival in the continuous presence of CDDP, ∼1000 cells were seeded in 6-well plates in triplicate. For tet-inducible expression of GFP-SLX4 (WT or mutant) or RNF168, Doxycycline (Dox) was added. After culturing for 2 weeks (TKFA-45) or 10 days (HCT116), cells were fixed with 100% ethanol, stained with crystal violet (0.006% crystal violet/25% methanol), and colonies were counted. For survival assays of TKFA-45 in the presence of MMC, cells were treated with the indicated concentrations of MMC for 24 h and then re-plated into fresh media.

Cell cycle analysis

Cells were treated with MMC (200 nM for TKFA-45(EHT) or 15 nM for HCT116) for 48 h and fixed in 70% ethanol for 30 min on ice. Fixed cells were stained with propidium iodide (10 μg/ml, nacalai tesque) in PBS containing RNase A (100 μg/ml, Invitrogen). Data were acquired using a FACSCalibur or FACSCantoII and analyzed with CellQuest Pro or FACSDiva software (BD).

Immunoprecipitation and western blotting

Cells were lysed with MCLB (50 mM Tris-HCl, pH 7.5, 150 mM NaCl, and 0.5% Nonidet-40 supplemented with protease inhibitors (cOmplete Protease Inhibitor Cocktail Tablets, Merck) and phosphatase inhibitors). Approximately 450 μg protein extract was incubated with 40 μL of anti-GFP magnetic beads (MBL) for 1 h. After washing five times, the immunoprecipitates were resuspended with Laemmli sample buffer. For immunoblotting of whole cell extracts, cells were washed once with PBS, and lysed in Laemmli sample buffer. Samples were separated by SDS-PAGE and transferred to a PVDF membrane (Millipore). Detection was performed as described previously (Unno et al., 2014).

Chromatin tethering assay using a LacR-LacO array system

U2OS 2-6-3 cells carrying an integrated LacO array were transiently transfected with mCherry-LacR-RNF168, GFP-SLX4-N, or control vectors and fixed on the next day. Alternatively, cells were simultaneously transfected with mCherry-LacR-RNF168 and siSLX4, fixed 24 h later, and stained with anti-SLX4 or anti-FK2 antibodies. Cells were observed, and foci were scored by an IN Cell Analyzer 2000 or a BZ-9000 fluorescence microscope.

ICL tracks by TMP and UVA micro-irradiation

MCF7 cells stably expressing GFP-SLX4-N and variants were first treated with TMP (2 μM 30 min) and irradiated with a PALM UVA laser (Zeiss) at 35% of the maximum power as described (Wu et al., 2016). Fluorescence intensity in the region of interest was chased until 20 min, and quantified using ImageJ software.

PLA of SLX4 and ICL by the Dig-TMP/UVA system

HeLa cells were transfected with indicated siRNAs, and 48hr later, cells were replated in 96-well black plates. HCT116 cells and derivatives were grown in the plates which were pre-coated with 100 μg/mL poly-L-lysine (nacalai tesque). Within 24hr, cells were treated with 20 μM Dig-TMP for 30 min and irradiated with 3 J/cm^2 UVA by a UV crosslinker equipped with 365nm UVA tubes (UVP, CL-1000). Then Dig-TMP was removed and cells were recovered in the absence of Dig-TMP. 1hr later, cells were fixed with 3% paraformaldehyde/2% sucrose solution containing 0.5% Triton X-100 for 30 min on ice, and permeabilized with 0.2% Triton X-100/PBS for 5 min. PLA was done by using Duolink PLA technology (Sigma-Aldrich) following the manufacture's instruction as described (Zhang et al., 2020).

Generation of RNF168 knockout HCT116 cells

The strategy for generation of RNF168 knockout HCT116 cells is described in Figure S6. A gRNA targeting the RNF168 RING domain was cloned into a CRISPR/Cas9 expression plasmid (GeneArt™ CRISPR Nuclease vector, Invitrogen). The gene targeting vector was constructed by cloning ~200 bp RNF168 genomic regions on both sides of the neomycin resistance gene cassette in pBluescript plasmid. Both vectors were simultaneously introduced into HCT116 using Lipofectamine 3000 (Invitrogen) and neomycin-resistant cells were selected. Targeted clones were identified by genomic PCR and verified by western blotting. Complementation of the knockout clone was done using lentiviral expression as previously described (Inano et al., 2017).

QUANTIFICATION AND STATISTICAL ANALYSIS

Quantification of subnuclear foci number or fluorescent intensity were done using IN Cell Developer Toolbox software following the manufacturer's instructions unless specified otherwise. Statistical significance was calculated by the Mann-Whitney test, one-way ANOVA or two-way ANOVA with a post hoc test for multiple comparisons using GraphPad Prism (version 5 or 8). Two or three independent experiments were done in triplicate and representative results are shown. Lines in dot plots indicate medians and interquartile ranges unless stated otherwise. Error bars in bar graphs indicate SD of more than three independent experiments.
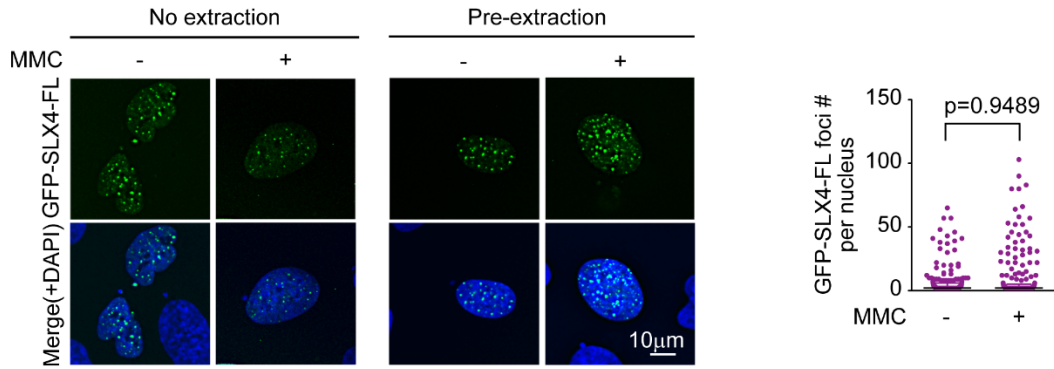
Cell Reports, Volume *37*

Supplemental information

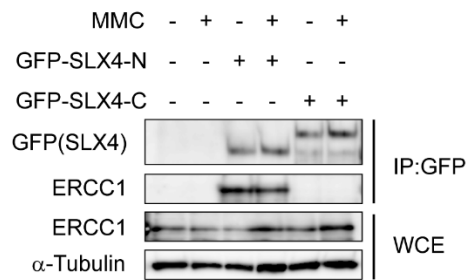RNF168 E3 ligase participates

in ubiquitin signaling and recruitment

of SLX4 during DNA crosslink repair

Yoko Katsuki, Masako Abe, Seon Young Park, Wenwen Wu, Hiromasa Yabe, Miharu Yabe, Haico van Attikum, Shinichiro Nakada, Tomohiko Ohta, Michael M. Seidman, Yonghwan Kim, and Minoru Takata
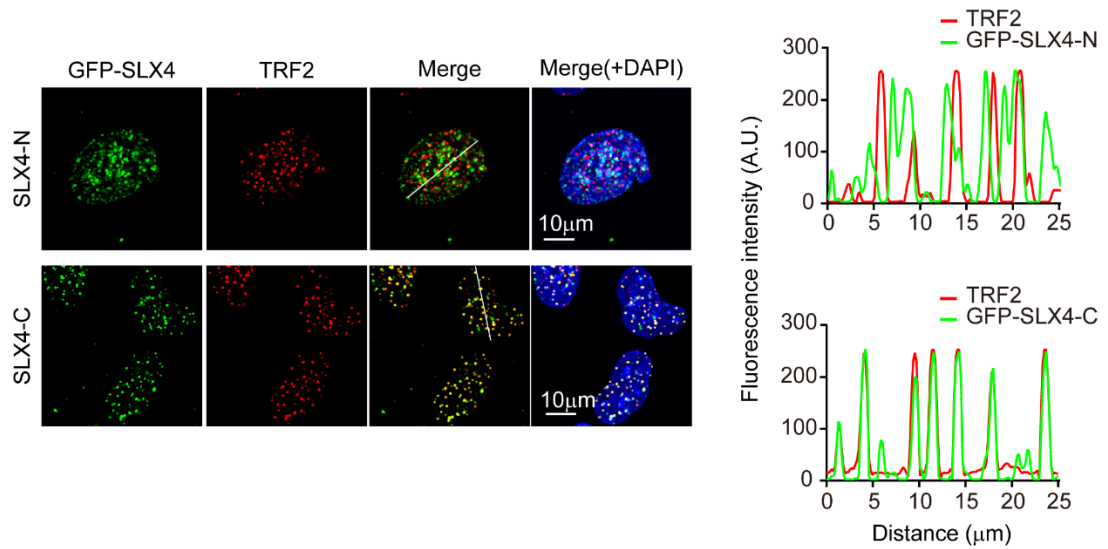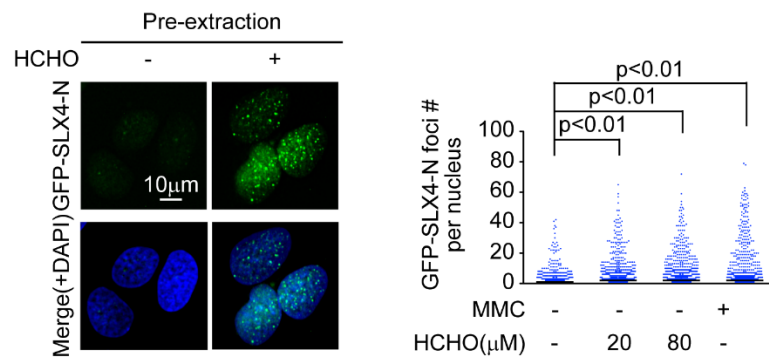
Figure S1. Subnuclear localization of GFP-SLX4-FL (full length), Related to Figure 1. (A) Foci formationof GFP-SLX4-FL (full length) expressed in U2OS cells. U2OS cells expressing GFP- SLX4-FL were treated with MMC and fixed with or without pre-extraction. Representative images and quantification of the number of foci per nucleus, with medianand interquartile range, are shown. More than 150 pre-extracted cells were scored. P-values were calculated by the Mann-Whitney test. **(B)** Interaction between SLX4 and ERCC1. U2OS cells expressing GFP-SLX4-N or GFP-SLX4-C were treated with or without MMC, then lysed. GFP-SXL4-N and GFP-SLX4-C were immunoprecipitated and probed with the indicated antibodies. WCE, whole cell extract. **(C)** Colocalization of MMC-induced foci of GFP-SLX4-N or -C stably expressed in U2OS cells with telomeres (detected by anti-TRF2). Representative images (**left**) and fluorescence intensity profiles across nuclear regions indicated by white lines (**right**) are shown. **(D)** Foci formation ofGFP-SLX4-N stably expressed in U2OS cells. Cells were stimulated with or without formaldehyde (HCHO), and fixed with or without pre-extraction. Representative imagesand quantification of the number of foci per nucleus, with median and interquartile range,are shown. More than 500 pre-extracted cells were scored. P-values were calculated by one-way ANOVA with multiple comparison. As a positive control, cells were treated with MMC (100 ng/ml for 24 h) and processed in parallel.
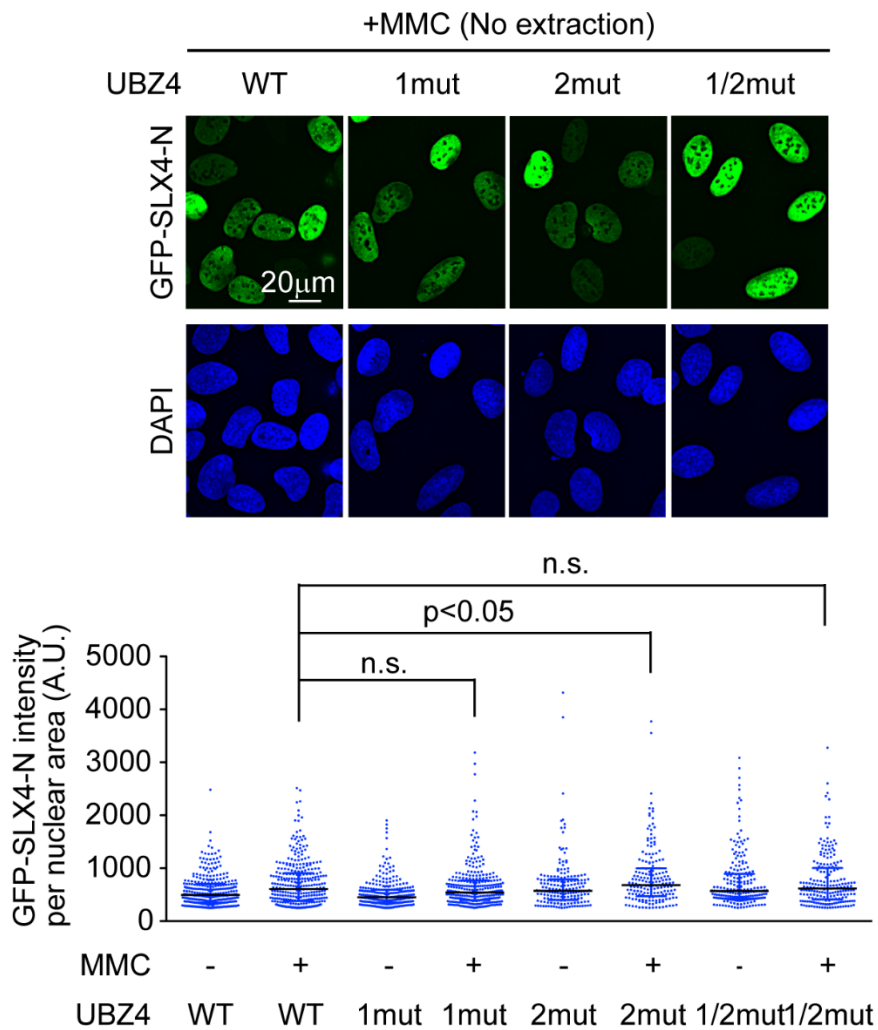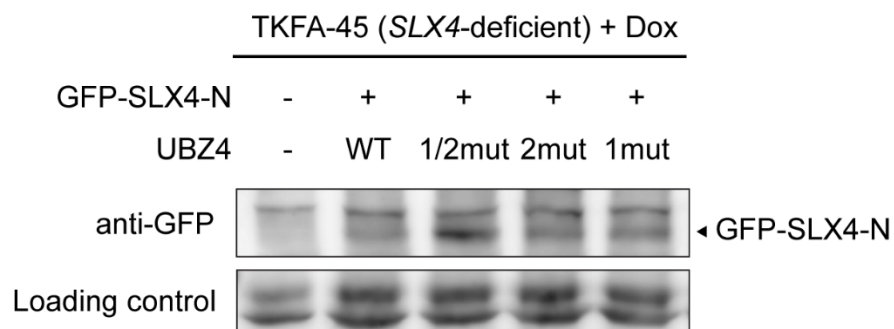
Figure S2. Expression of GFP-SLX4-N UBZ4 mutants in U2OS cells, Related to Figure 2. (A) Expressionlevels of the indicated GFP-SLX4-N variants introduced into U2OS cells. Representative images and quantification of GFP fluorescence levels in nuclei are shown. **(B)** Expressionlevels of the indicated GFP-SLX4-N variants introduced into TKFA-45/E6E7/hTERT cells. Cells were lysed and analyzed by western blotting.
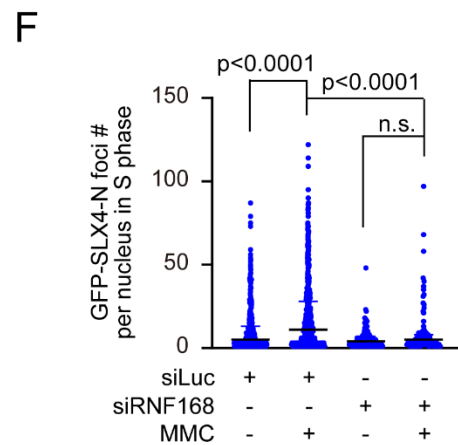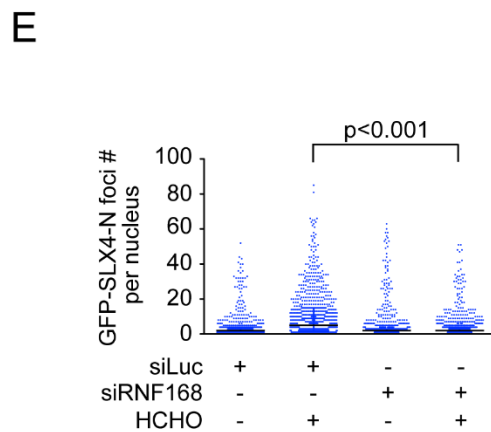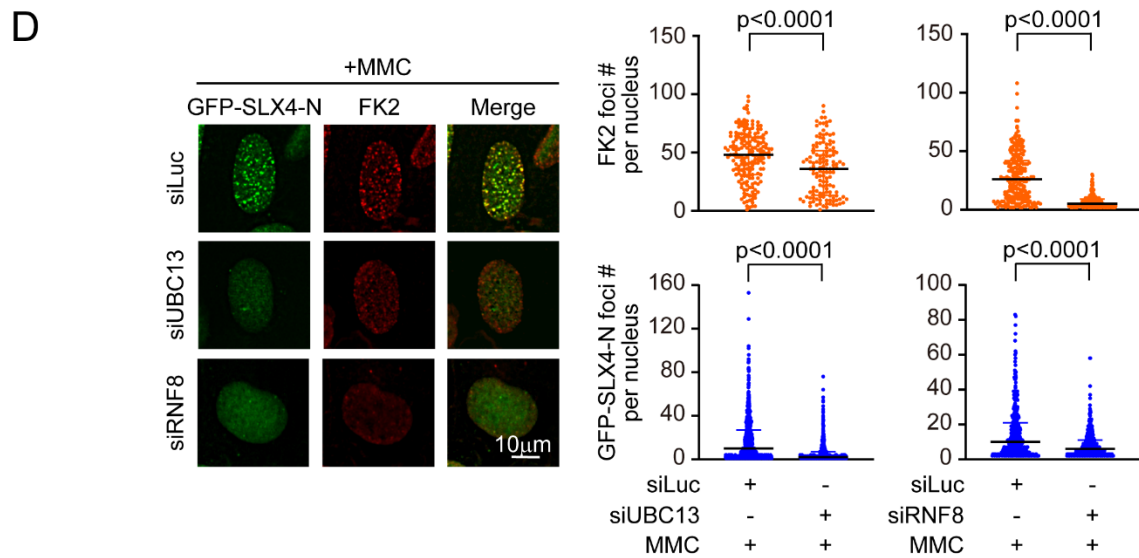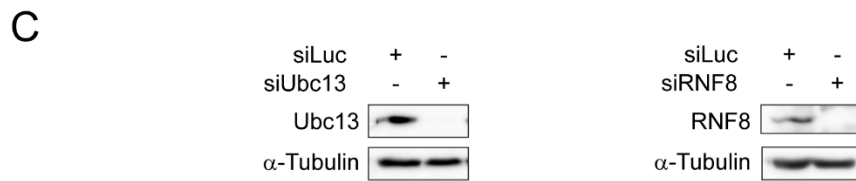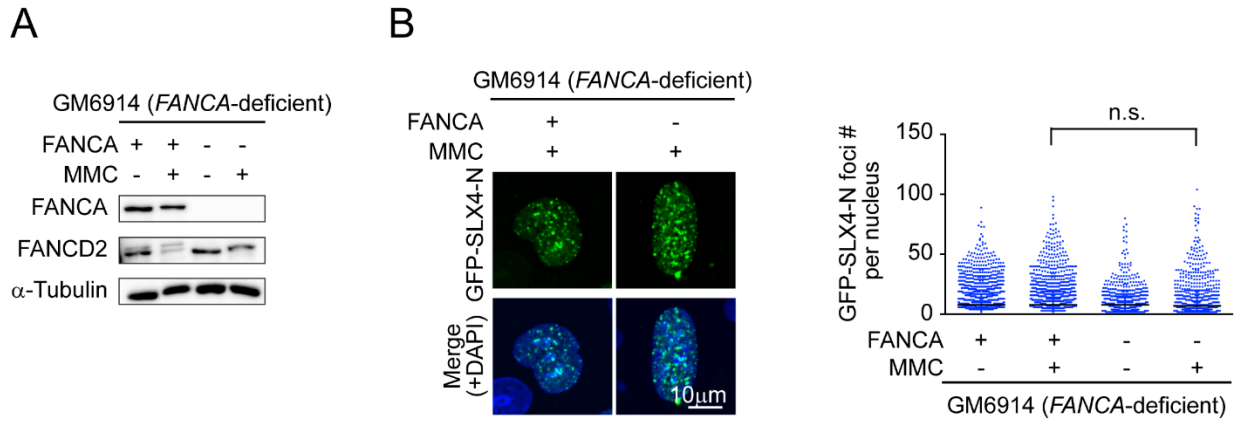
**Figure S3. SLX4-N foci formation is dependent on RNF168 and UBC13 but not on FANCA, Related to Figure 3 and 4. (A)** GM6914 cells with or without FANCA complementation were stimulated with MMC (100 ng/ml for 24 h) and verified by western blotting using anti-FANCA or FANCD2 antibodies. **(B)** Effects of *FANCA* deficiency on GFP-SLX4-N foci formation. Cells in (A) were transfected with the GFP-SLX4-N expression vector, treated with or without MMC, pre-extracted, and fixed. Representative images and quantification of thenumber of foci per nucleus, with median and interquartile range, are shown. More than 500 cells were scored. P-values were calculated by one-way ANOVA with a post hoc test.

(C) U2OS cells expressing GFP-SLX4-N were transfected with siUBC13 or siRNF8, and the depletion was verified by western blotting. **(D)** UBC13- or RNF8-dependent GFP-SLX4-N foci colocalized with ubiquitin foci. The siRNA transfected cells, as in (C), were treated with MMC (100 ng/ml, 24 h), and stained with anti-FK2 antibody. Representative imagesand quantification of FK2 or GFP-SLX4-N foci by an IN Cell Analyzer2000 are shown.Median and interquartile range from more than 100 cells were scored. P-values were calculated by the Mann-Whitney test. **(E)** Formaldehyde-induced RNF168-dependent GFP-SLX4-N foci. U2OS cells expressing GFP-SLX4-N were transfected with siRNF168, and 48 h later, stimulated with formaldehyde (HCHO, 80 μM for 24 h). Quantification of GFP-SLX4-N foci is shown with median and interquartile range. More than 500 cells were scored by an IN Cell Analyzer 2000. P-values were calculated by one-way ANOVA with a post hoc test. **(F)** MMC-induced GFP-SLX4-N foci were decreased by siRNF168 in S phase cells as defined by positive anti-PCNA immunofluorescence ("replication foci"). U2OS cells expressing GFP-SLX4-N were transfected with siRNF168, and 48 h later, stimulated with MMC. Pre-extracted cells were stained by anti-PCNA, and the images were captured by IN Cell Analyzer2000. Cells showing PCNA density (intensity per pixel) higher than 650 A.U. were defined to be in the S phase. Quantification of GFP-SLX4-N foci was shown. Median and interquartile range from more than 95 cells were scored. P-values were calculated by one-way ANOVA with a post hoc test.
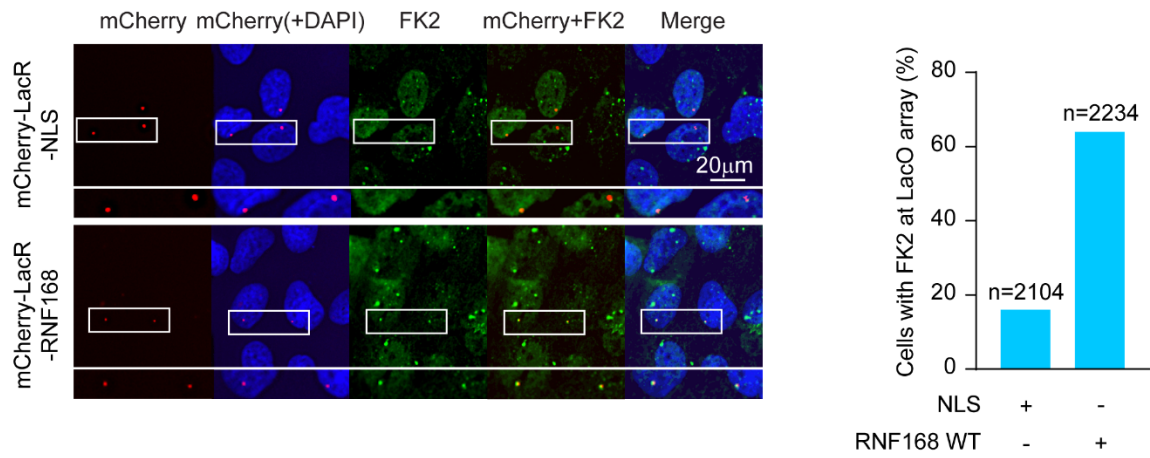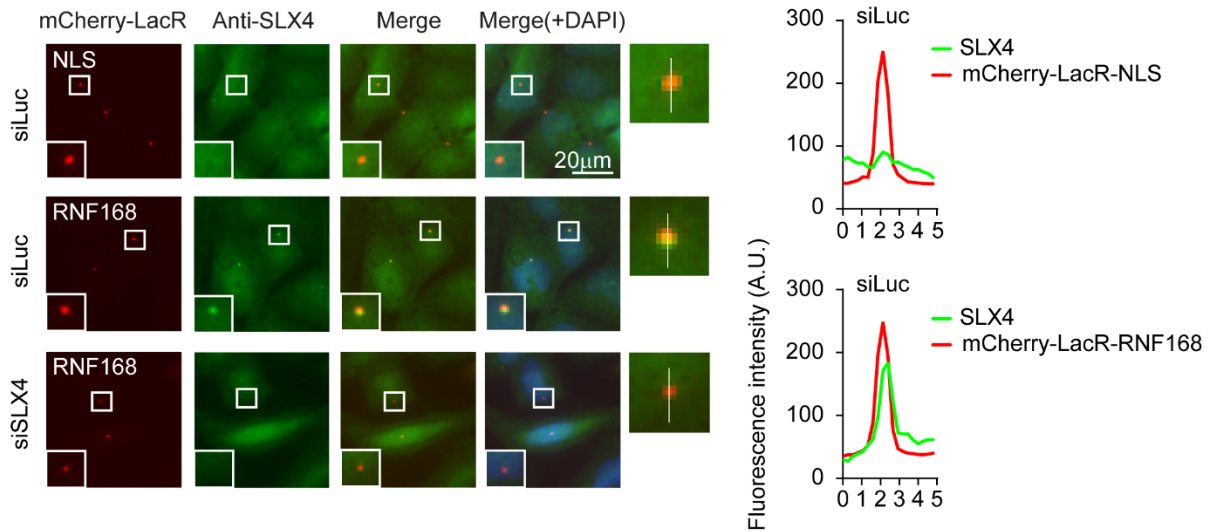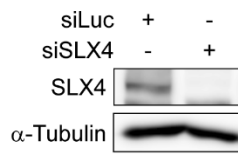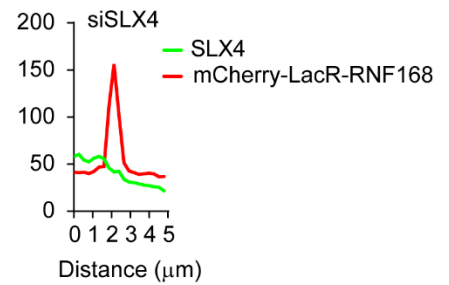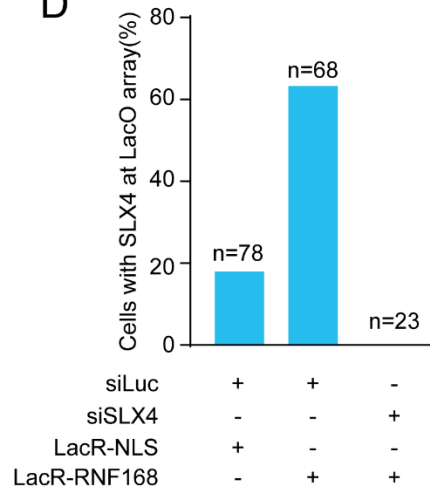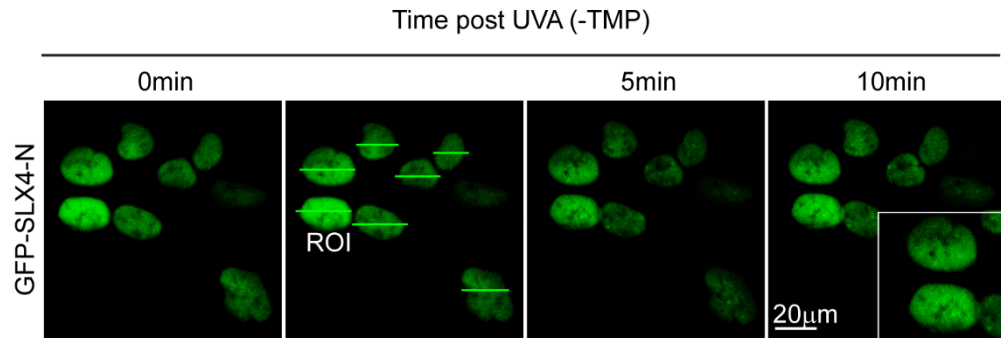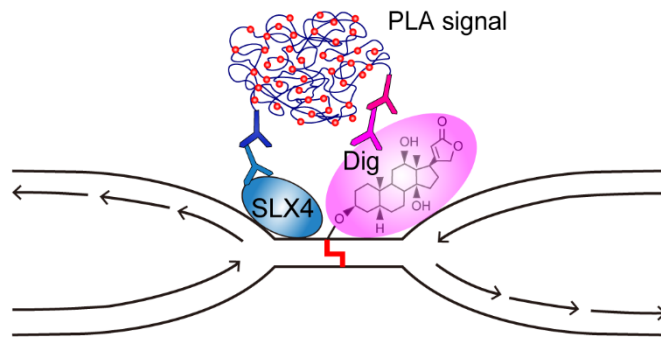
Figure S4. Accumulation of ubiquitin or SLX4 at a LacO array by chromatin- tethered RNF168, Related to Figure 5. (A) mCherry-LacR-RNF168 foci at a LacO array and colocalizing ubiquitin foci. U2OS 2-6-3 cells carrying an integrated 256x LacO array were transientlytransfected with a vector expressing mCherry-LacR-fused RNF168 or negative control LacR-NLS (nuclear localization signal). 24 h later, cells were stained with anti-FK2 antibody. Representative images and the percentage of cells with positive FK2 signals atmCherry-positive the LacO array are shown. **(B)** mCherry-LacR-RNF168 foci at the LacOarray and colocalizing SLX4 foci. U2OS 2-6-3 cells were treated with siSLX4 or siLuc, and then transiently transfected with a vector expressing mCherry-LacR-fused RNF168 or a negative control LacR-NLS (nuclear localization signal). 24 h later, cells were stainedwith anti-SLX4 antibody. Representative images (left) and fluorescence intensity profilesof mCherry-LacR-RNF168 and SLX4 signals within a focus (corresponding to the LacOarray) traced by a white line are shown. **(C)** SLX4 depletion was verified by anti-SLX4 western blotting. **(D)** Percentages of cells with positive SLX4 signals at the mCherry- positive LacO array. Quantification of the foci in captured images were carried out by ImageJ. Cells with higher peak SLX4 signals at the mCherry foci than those in SLX4- depleted cells were regarded as positive for SLX4. Numbers of cells scored are indicated at the top of each bar.

A

Time post UVA (-TMP)

| 0min | 5min | 10min |

GFP-SLX4-N

ROI

20μm

B

PLA signal

Dig

SLX4

C

| UVA only | Dig-TMP + UVA | | |

siRNA | Luc | Luc | SLX4 | RNF168

10μm

siLuc	+	-	-
siSLX4	-	+	-
siRNF168	-	-	+

SLX4
RNF168
α-Tubulin

p<0.0001

p<0.0001   n.s.

SLX4-Dig PLA signal per nucleus

20μM Dig-TMP	-	+	+	+
3J/cm² UVA	+	+	+	+
siRNA	Luc	Luc	SLX4	RNF168
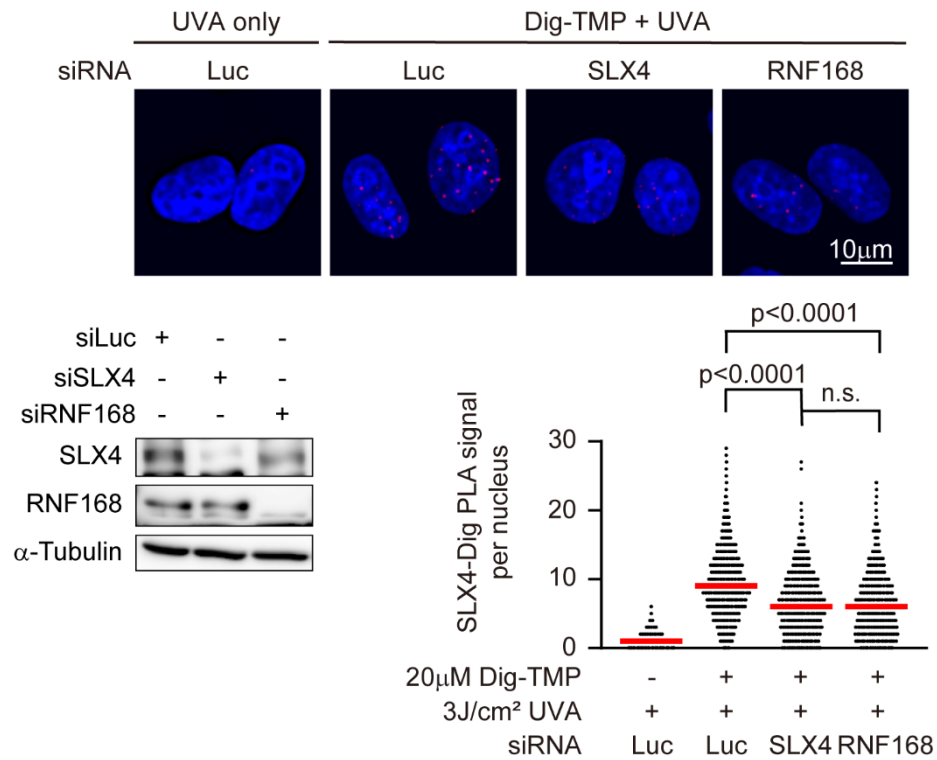
Figure S5. DNA damage induction by laser micro-irradiation, Related to Figure 5. (A) Absence of appreciableeffects by the UVA laser irradiation on GFP-SLX4-N WT distribution in U2OS cells without pretreatment with trimethylpsoralen (TMP). The same set of MCF7 cells ex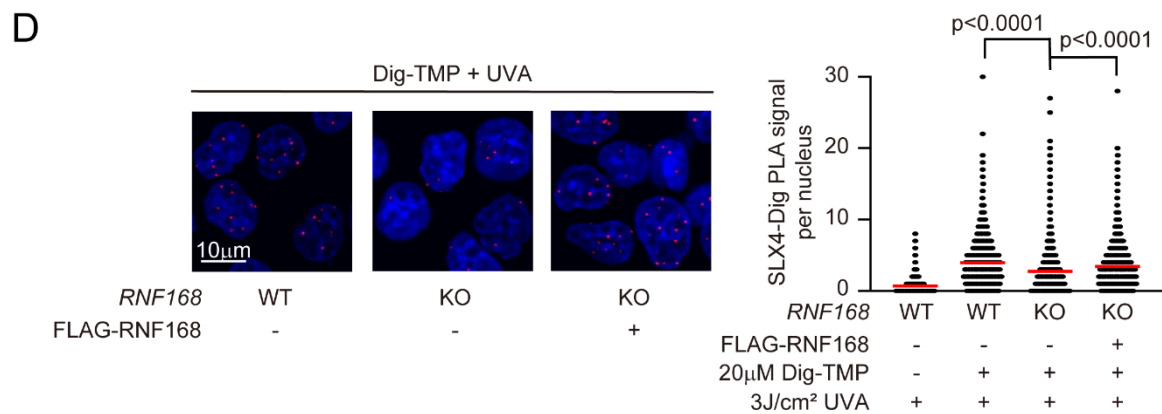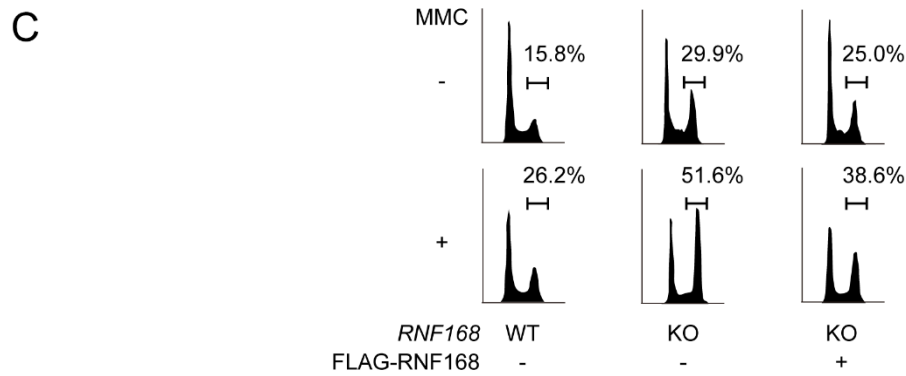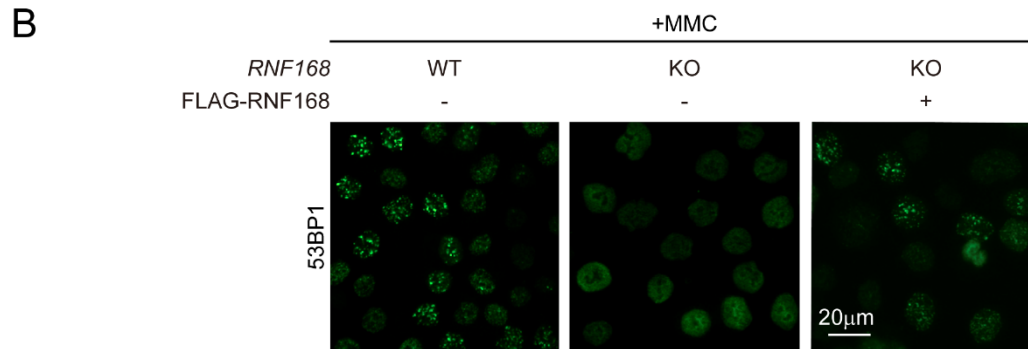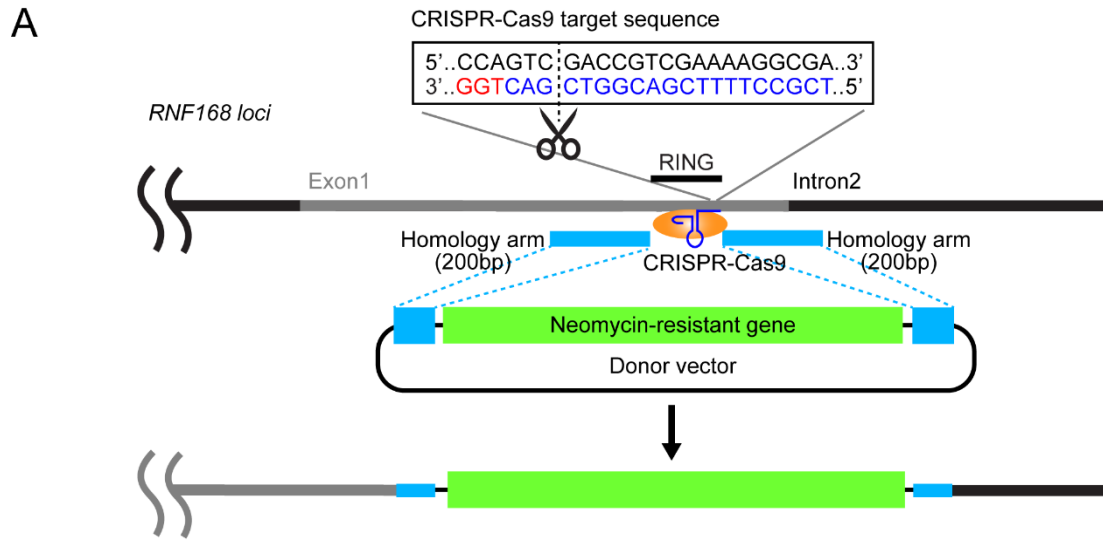pressing GFP-SLX4-N were chased over 10 min following the irradiation. The green lines in the second image from the left indicate the laser-irradiated region of interest (ROI). **(B)** An experimental scheme of the Digoxigenin (Dig)-TMP/UVA system and PLA to detect recruitment of SLX4 to induced ICL. ICL is formed with incorporated Dig-TMP following UVA irradiation. SLX4 and Dig are detected by the respective antibodies and the PLA signals are generated between the oligonucleotide-labelled secondary antibodies by the rolling circle amplification. **(C)** PLA between anti-Dig and anti-SLX4 in HeLa cells. HeLa cells were treated with control siRNA (Luc) siSLX4, or siRNF168 and incubated with or without Dig-TMP then irradiated with UVA. Representative images (**upper**), verification of siRNA by western blotting (**lower left**), and quantitation of PLA signals per nucleus (**lower right**) are shown. Red lines indicate the mean value and P-values were calculated by one-way ANOVA with a post hoc test. Images of more than 1000 cells were automatically captured by IN Cell Analyzer 2000 and scored by the Developer toolbox software.

A

CRISPR-Cas9 target sequence

5'..CCAGTC GACCGTCGAAAAGGCGA..3'
3'..GGTCAG CTGGCAGCTTTTCCGCT..5'

RNF168 loci

B

+MMC

RNF168	WT	KO	KO
FLAG-RNF168	-	-	+

53BP1

20μm

C

MMC			
-	15.8%	29.9%	25.0%
+	26.2%	51.6%	38.6%
RNF168	WT	KO	KO
FLAG-RNF168	-	-	+

D

Dig-TMP + UVA

RNF168	WT	KO	KO
FLAG-RNF168	-	-	+

10μm

p<0.0001   p<0.0001

SLX4-Dig PLA signal per nucleus

RNF168	WT	WT	KO	KO
FLAG-RNF168	-	-	-	+
20μM Dig-TMP	-	+	+	+
3J/cm² UVA	+	+	+	+

Figure S6. Generation of RNF168 knockout HCT116 cells, Related to Figure 6. (A) A schematic of *RNF168*gene disruption executed by CRISPR-Cas9 in HCT116 cell line. A targeting vector and configurations of thetargeted RNF168 region are shown. **(B)** MMC-induced 53BP1 foci formation in HCT116wild type (WT) cells were abrogated in the RNF168 knockout (KO). HCT116 RNF168 KO cells were lentivirally complemented with *RNF168*. The RNF168 expression was verified by western blotting (**Figure 6A**). Cells were stimulated with MMC and stained with anti-53BP1 antibody. **(C)** Cell cycle distribution of wild type, *RNF168* KO, or the KO cells complemented with FLAG-RNF168. Cells were treated with or without MMC (15 nM for 48 h) and stained with PI. The percentage of cells in G2 phase was indicated. **(D)** The SLX4 recruitment to Dig-TMP/UVA-induced ICL as detected by PLA with anti-Dig and anti-SLX4 antibodies in WT, KO, and the complemented KO cells. Representative images (**left**) and quantitation of PLA signals per nucleus (**right**) are shown. Red lines indicate mean value and P-values were calculated by one-way ANOVA with a post hoc test. Images of more than 1500 cells were automatically captured by IN Cell Analyzer 2000 and scored by the Developer toolbox software.